Transactions of NAMP 24, (2026) 21-52

Transactions of
The Nigerian Association of
Mathematical Physics
Journal homepage: https://nampjournals.org.ng

INTEGRATION AND JUXTAPOSITION OF EULER AND WERNER DECONVOLUTION TECHNIQUES FOR LITHO-STRUCTURAL CONTACT IDENTIFICATION AND MAGNETIC BASEMENT DEPTH DETERMINATION: A CASE STUDY OF ADO-EKITI, SOUTH-WEST NIGERIA

Ishola S.A

Department of Earth Sciences, Olabisi Onabanjo University Ago-Iwoye, P.M.B 2002, Ago-Iwoye, Ogun State, Nigeria

ARTICLE INFO

Article history:
Received xxxxx
Revised xxxxx
Accepted xxxxx
Available online xxxxx

Keywords:
Euler deconvolution, dykes, tensor, models, gridded, aeromagnetic.

ABSTRACT

The study applied high-resolution aeromagnetic data for the characterization and consequent delineation of geological structures of Ado-Ekiti (sheet 244) and its environs in southwestern Nigeria. The principle of tensor Euler deconvolution was harnessed for the interpretation. The acquired data were processed using Excel package and Geosft Oasis Montaj 8.4v to model the subsurface topography. Euler Deconvolution (ED) showed the minimum depth of 132.2m and maximum depth of 2233.9m for shallow and deep magnetic sources, Werner Deconvolution (WD) were used to confirm magnetic anomalies and corresponding intrusive contacts like dykes and sills. The output from Euler deconvolution was associated with dykes with deeper depth range of 132.2 beneath mean sea level. This study has therefore proven that the integration of Euler and Werner deconvolution techniques on the aeromagnetic data is valuable in the characterization of the subsurface geological structures delineation/ contact identification of most of the encountered structures in the area.

1. INTRODUCTION

The Earth's subsurface is a complex and dynamic system that holds valuable information about its geological history, mineral resources, and structural composition. Geophysical methods, particularly magnetic surveys, have proven to be effective tools for investigating subsurface structures, especially in basement complex terrains [1]. Magnetic surveys measure variations in the Earth's magnetic resulting from the impacts of magnetic minerals in the rocks, providing insights into the depth and geometry of magnetic sources [2]. Magnetic surveys explore the subsurface geology due to the corresponding anomalies in the Earth's magnetic field particularly from the magnetic properties of rocks below the earth surface.

*Corresponding author: ISHOLA S.A
E-mail address: ishola.sakirudeen@oouagoiwoye.edu.ng
https://doi.org/10.60787/tnamp.v24.667

The delineation of depth to basement rocks and corresponding surface mapping of the topographic are accomplished through these techniques. Hence, structures and depths to basement rocks are delineated and mapped using field magnetic data in accurate manners [3]. Integrating Euler deconvolution and Werner Filtering (Werner deconvolution in geophysical in Geophysical context) enhances magnetic exploration by using Euler for fast, semi-automatic depth estimation and source location from potential field data, while Werner filtering optimizes the data by removing noise and isolating the residual anomalies that Euler deconvolution requires. This synergy provides more accurate and reliable basement depth maps and geological insights by addressing limitations inherent in each technique, leading to improved interpretations of subsurface structures and better targeting for resource exploration [4−12]. There are numerous benefits of the integration and juxtaposition of Euler deconvolution and Werner deconvolution in geophysical investigation. Werner filtering effectively removes noise and separates regional background fields from the residual anomalies that significantly beneficial in exploration studies, providing cleaner input data for Euler deconvolution [13−15]. By focusing on the signal of interest, the integrated approach leads to enhanced source delineation by focusing on the signal of interest, by creating allowance for more precise identification of geological sources like faults, dykes, and intrusive bodies. It creates opportunities for the provisions of more reliable depth estimates as the input data processed by Werner filtering leads to more coherent and accurate depth solutions from the Euler deconvolution, giving clearer picture of the magnetic basement [16−17]. It leads to a detailed and comprehensive interpretations of he acquired data by providing both the depth to magnetic sources from Euler solution and the geological context from Werner-filtered data, leading to a more complete organization of the geometry of the subsurface structure [18]. Euler deconvolution and Werner Filtering have over the years served as complementary tools in data preprocessing and processing as Wiener filters were used to estimate the background field and the noise within the observed magnetic data [4, 19−52]; the filter's output, after removing the background and noise, is a residual anomaly map [53]; the residual map outlines and pinpoints the observed anomalies caused by shallow geological structures and the magnetic basement, which is essential for accurate depth estimation [54−55]. Euler deconvolution technique has been highly instrumental in depth estimation. It processes the residual anomalies for the determination of location and the corresponding depth of magnetic sources [56−57], it uses the relationship between the magnetic field data and its consequent derivatives to provide a semi-automatic solution [58−67], the solutions from Euler deconvolution are windowed and filtered to remove spurious solutions and ensure the accuracy of the final depth models [65−67].

The integration Euler deconvolution and Werner Filtering has been of immense geological insights because it allows for a better understanding of subsurface structures [68−70], it can reveal different basement depths, identifying shallower sources that might indicate areas of mineralization or deeper sources that define the overall basin structure [71−72]. Also, this integrated analysis supports broader geological mapping and aids in identifying areas with potential for resource deposits [73−74]. Furthermore, the integration of Euler and Werner deconvolution enhances litho-structural identification, improves contact location accuracy, and refines magnetic basement depth estimations leveraging each method's strength; Euler deconvolution a structural index-based technique, excels in locating 2D and 3D sources with variable depths and provides a measure of source shape., while Werner deconvolution , a profile biased method, is effective for determining depths to individual sources particularly thin dykes, based on a polynomial fit. Euler's integration with Werner deconvolution can reduce the profile-bias Werner and account for the varying source shapes that Euler deconvolution can identify, thus providing more reliable results than either method alone [75−79]. The impact of the integration can be observed in improved litho-structural identification where the combination of Euler's ability to delineate faults and sources of varying structural indices with Werner's sensitivity to individual contact can help map complex geological

structures with greater confidence [80−88]; it provides an enhanced contact location since Werner deconvolution is excellent at identifying contacts, especially for thin dykes, whereas Euler deconvolution can make possible provision for location and associated depth information for sources with different shapes, such as contacts and faults. The integration allows for a more comprehensive identification of lithological boundaries [86−88]; it provides more reliable magnetic basement depth because Euler deconvolution estimates source depths with a structural index allowing for different source shapes, while Werner deconvolution provides a detailed depth estimate for simpler 2D sources. Their integration can improve reliability of depth estimations by validating findings and covering the limitations of each method [89−90]. In terms of method and application, Euler deconvolution solves a system of equations relating field gradients to the location and depth of magnetic sources, and a structural index (SI) applicable to 2D and 3D data while Werner deconvolution fits a polynomial to the observed magnetic field data and its derivatives, based on the assumption of thin, isolated sources primarily designed and applicable for 2D profile Data. In terms of source shapes, Euler deconvolution accounts for various source shapes like dykes, faults, contacts, prisms using the structural index and the output provides source locations (x, y, z), depth, and a structural index value while Werner deconvolution is best suited primarily for thin sheets and dykes or sources composed of multiple thin dykes and the corresponding outputs yield a more detailed depth estimation to a source based on a best-fit polynomial. Based on window biasness, Euler deconvolution is more resistant to window size variation but can be sensitive to poor structural index choices while Werner deconvolution is more sensitive to data window size and the presence of nearby sources. Certain technical conditions are considered before Euler deconvolution and Werner deconvolution can be integrated in field potential gradient studies; when both 2D and 3D geological structures are present, Euler deconvolution can provide a broader picture, while Werner deconvolution can be used to detail the depths and boundaries of specific 2D features [91−93]; findings can be validated from one method by cross-referencing with the results of the other [94]; for mineral exploration and engineering projects where accurate mapping of faults, basement depth, and sedimentary thickness is crucial [95−101].

The need to map the depth to the basement in Ado Ekiti and its environs has become more crucial due to urbanization, infrastructural development, and the potential for discovering mineral resources. Delineation and mapping of the basement depth provides a critical and significant field information of the depth at which the basement rocks lie beneath the overlying sedimentary layers. This study aimed at determining depth to the magnetic basement using magnetic survey data cum depth estimation of the causative bodies in Ado Ekiti and its environs using the combined effects of Euler and Werner Deconvolutions.

STUDY AREA

Location and Accessibility

Ado-Ekiti Local Government Area is bounded on the North and West by Ifelodun/Irepodun Local Government Areas while other neighbouring towns like Aiyekire, Ikere, and Ekiti South-West Local Government Areas are found on the East and South. The area is generally accessible by major and minor roads, as well as footpaths, facilitating easy navigation for surveying, though the condition of some federal roads in the state can pose challenges [102].

Physiography and Geology of the Study Area

Ekiti State is located between longitude 4^0 5’ and 5^0 45’ East of the Greenwich meridian and between latitude 7^o 15’ and 8^o 5’ North of the equator. The state is largely situated on an upland zone, rising well above the mean sea level with over 250m. On the general overview of the outlay, the study area possesses an undulating land surface area with a conspicuous landscape that is principally characterized by old plains

divided by steep-sided out-cropping dome rocks whose field occurrence are displayed in single fashion while others appear in groups or clusters of ridges. Ekiti State and its environs is typically a tropical climate characterized by two seasons that are of distinct representations, which are the wet season that runs from April to October and the dry season that runs from November to March. The topographic feature of the study area is predominantly an undulating plain with elevations whose approximate values above sea level varying from 200m in the southeast to 500m in the northeast. The prominent steep-sided outcropping dome rocks that punctuated the landscape is often referred to as inselbergs. The area forms the source of several streams, including Amu, Awedele, Ajilosun, and Adere. River Ajilosun, for instance, flows in a North-East to South-West direction and contributes to the larger Ogbese drainage basin [102].

The geologic framework and subsequent attributes of the area is typical of the migmatite gneiss complex rocks emanating from the Precambrian Basement Complex of southwestern Nigeria, it is comprised of different rocks and associated mineral assemblages namely undifferentiated granite, charnockitic rocks, gneisses, schist/quartz schists. migmatite gneiss rocks, porphyritic biotite-hornblende granite, alongside the superficial deposit of clay and quartzite, medium to coarse granite which are often associated with mineral resources and groundwater potential potentials of the area (Figure 1). The resultant effect of the association of the fine-grained charnokite and the porphyritic biotite-hornblende granite gives a suggestive outcome of a common age [103]. One of the notable area that serves as a miniature of the geology of southwestern Nigeria is Ado-Ekiti because the generality of the rocks in southwestern Nigeria with the exception of the schistose rocks are found in Ado-Ekiti. The Migmatite-quartzite complexes ranking as the oldest rocks into which other rocks (older granite, charnokite, aplite and quartz veins) later got intruded. During the Pan-African orogeny, the charnokites and the older granites intruded into these host rocks. Well over 60% of the study area is covered by Migmatite-gneiss (Figure 1) and was later intruded by other rocks in successions. The occurrence and representation of Migmatite rock exposures is in form of highly denuded hills essentially comprised of fine textures. The mafic portion of the rocks are principally composed of biotite, hornblende and opaque minerals while quartzo-feldspartic is a typical constituent of the felsic portion. The compositional variations displayed by the rock minerals is an indication of closely spaced alternating bands of leucocratic minerals (quartz and feldspars) and melanocratic minerals revealing the preponderance of biotite minerals. White to gray colourations exhibited by quartzite in the study area are typically due to varying iron-oxide in the rock. Good examples of massive quartzite outcrops with heights of 100m above the surrounding terrain are observed occur around the southwestern portion of the study area. Quartzite is highly resistant to chemical weathering and often constitutes ridges and resistant hilltops. The observed shape of the outcropped charnokitic hilly rocks either oval or semi-circular hills ranging between 5 and 10m high with abundance of granite boulders distributed in some other outcrops. **Ilara Mokin** and **Ipelu** feature schists, gneisses, dolerite, and granites, shaped by tectonic deformation and weathering, leading to lateritic soils and inselbergs. **Araromi, Ijare,** and **Italepo Oda** are dominated by high-grade metamorphic rocks like gneisses, schists, and granites, with prominent folds and fractures reflecting regional tectonics. **Ita Ogbolu** and **Ago-Binuyo** exhibit coarse-grained granites, foliated gneisses, and pegmatites, shaped by intrusive and metamorphic events**. Ise, Awodeyi,** and **Emure Ekiti** also lie within this complex and show similar lithological compositions and tectonic imprints, with variations in mineralization and metamorphism intensity. The region experiences a tropical climate with distinct wet (March–November) and dry (December–February) seasons, which accelerate weathering and influence soil formation. The geology across these locations reflects uniform Basement Complex characteristics, with implications for structural mapping, mineral potential, and geotechnical applications [102, 104−107]. The structural features like folds, faults, fractures, and shear zones found in the study area were typically due to the resultant effects of the shaping of the rock units during the Pan-African Orogeny (~600 Ma).

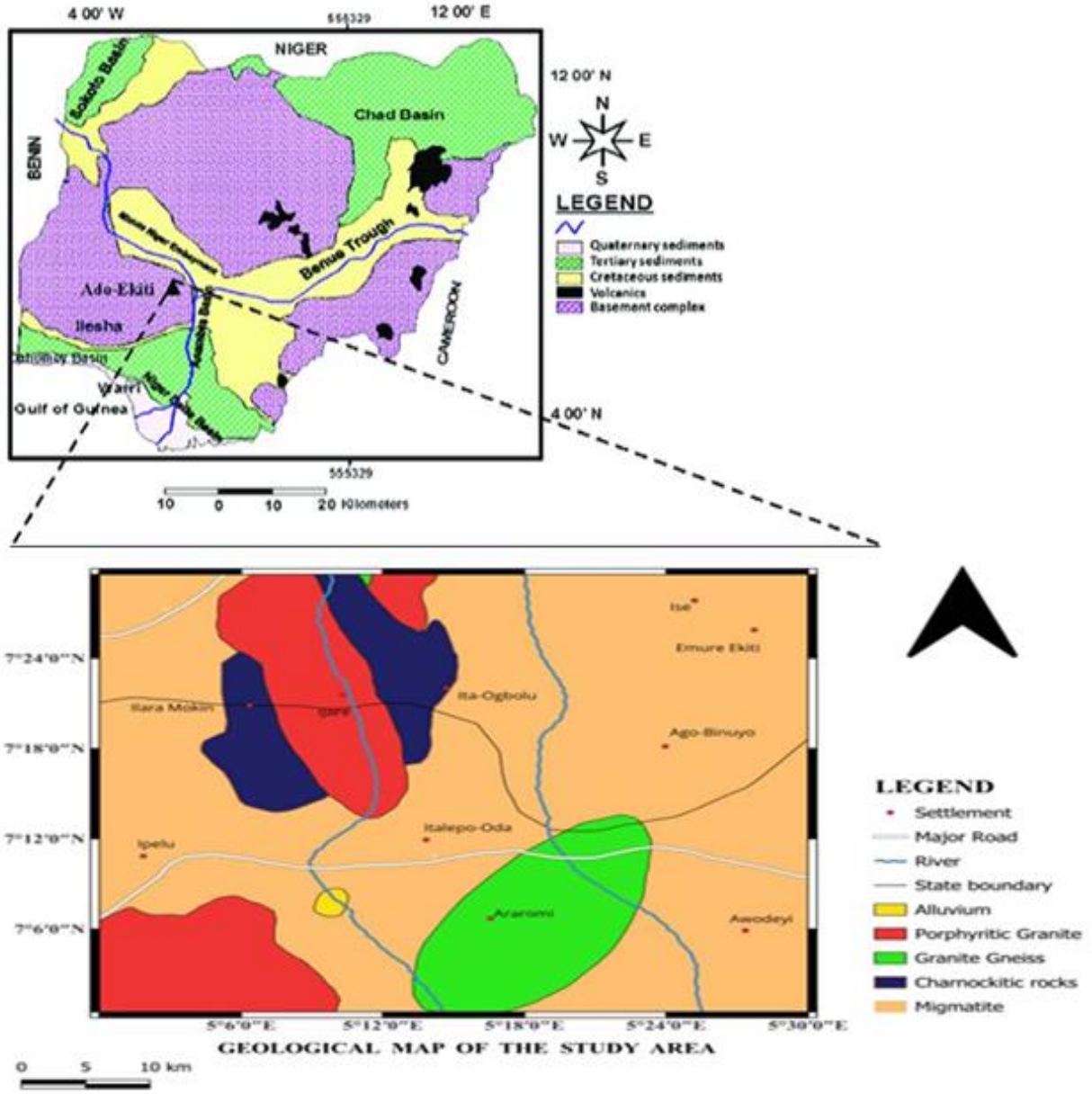

Figure 1: Inset map showing the Geology of the study area in connection with Nigeria Basement Complex [102]

MATERIALS AND METHODS

Theoretical Background and Modeled Formulation Techniques

Principles of Euler deconvolution

Euler deconvolution has been instrumental and applicable in different form to geophysical exploration studies involving gravity and magnetic for about sixty years. The principles of operations are based on Euler's homogeneity equation that was enunciated as far back as eighteenth century [108]. The documentation of Euler deconvolution principles can be traced back to the technical reports of [109] who earlier penned down Euler's homogeneity equation for the magnetic case and consequently derived the associated structural indices for a point pole and for a point dipole. The study of Euler deconvolution was enhanced by [110] who further understudied

and implemented the varying method of application of Euler deconvolution to modeled and real-time field acquired data along established profiles. This was accompanied by the work of [107] following up the suggestive publication of [110]; he developed the equivalent method operating on the gridded magnetic data otherwise known as 3D Euler deconvolution. The conceptual framework of the zero structural indexes for a contact was equally introduced and the Euler deconvolution was suggested as the recognized name. It was afterwards suggested that the method could be applied to gravity data and gravity gradient data. The varying applications of the conventional Euler deconvolution to gravity data and gravity gradient data have been undertaken by several auhors [102, 111−136]. However, most of the investigative research outcomes in these studies were centered on model simulation of the acquired data or the utilization of the three principal gravity gradients calculated from the computed vertical component of the observed gravity.

The Euler deconvolution technique can be harnessed for speed interpretation of any potential field data in terms of depth and geological structure. The basic conceptual framework of Euler deconvolution can be reviewed and tensor Euler deconvolution can be derived for gravity tensor gradient data

Conventional Euler deconvolution

Conventional Euler deconvolution (CED) utilizes three orthogonal gradients of any potential quantity as well as the potential quantity itself both for source locations and corresponding depth determination expressed in equation 1.

$$(f - f_0)Ц_{hf} + (g - g_0)Ц_{hg} + (h - h_0)Ц_{hh} = W(8_h - Ц_h) \quad (1)$$

considering the potential anomaly vertical component $Ц_h$ of a given body possessing a homogeneous gravity field as shown in equation 1, where f_0, g_0, and h_0 are the unknown co-ordinate systems of the source body centre or the estimated edge while the *f, g* and *h* are known co-ordinate systems of the observation point of the potential gradients. The values and $Ц_{hf}$, $Ц_{hg}$, and $Ц_{hh}$ are the measured potential gradients along the *f*–, *g*– and *h*– directions; W represents the structural index; and 8_h represents the regional value of the gravity to be estimated. Equation (1) can be modified to produce equation (2).

$$f_0Ц_{hf} + g_0Ц_{hg} + h_0Ц_{hh} + W8_h = fЦ_{hf} + gЦ_{hg} + hЦ_{hh} + WЦ_h \quad (2)$$

Four unknown parameters (f_0, g_0, h_0, 8_h) are identified in equation (2) and there are *n* number of observation data points available for the derivation of the four unknown parameters. When the number is configured to be greater than four (n > 4), these parameters can be estimated using Moore-Penrose inversion Scheme or equivalent techniques [108, 137].

Tensor Euler deconvolution

Tensor Euler deconvolution (TED) is inherently patterned for the consideration of the full potential gradient tensor and all components of the anomaly vector. It encompasses the conventional Euler equation (1) and utilizes two somewhat similar additional equations for the horizontal components are expressed in equation (3) and (4):

$$(f - f_0)Ц_{ff} + (g - g_0)Ц_{fg} + (h - h_0)Ц_{fh} = W(8_f - Ц_f) \quad (3)$$

$$(f - f_0)Ц_{gf} + (g - g_0)Ц_{gg} + (h - h_0)Ц_{gh} = W(8_g - Ц_g) \quad (4)$$

The values of $Ц_f$ and $Ц_g$ are the respective horizontal components of the potential vector along the f– and g– directions. If the horizontal component values are not available, these components can be derived from the vertical components or computed from the process of deconvolution. The list of values $Ц_{ff}, Ц_{fg}, Ц_{fh}; Ц_{gf}, Ц_{gg}, Ц_{gh}$ are potential tensor gradients. $ϑ_f$ and $ϑ_h$ are the regional values of the horizontal components to be estimated if values $Ц_f$ and $Ц_g$ are available, otherwise the quantities $(ϑ_f - Ц_f)$ and $(ϑ_g - Ц_g)$ can be further projected in the process. Therefore, *n* observation data points give rise to the product of 3 and *n* set of equations comprising of six unknowns (3*n*) but when n is found to be greater than 2 ($n > 2$), we can make calculation for the source position as well as the regional values using Moore-Penrose inversion scheme or its equivalent techniques. The merits of tensor Euler deconvolution is that all the measured tensor gradients are fully exploited and additional constraints are fashioned on the Euler solutions [108].

Application Euler deconvolution on different data types

CED technique can be applied to profile data with 2-D Euler using a mobile window of *n* equally spaced nodes or gridded data with 3D Euler using a window size of n×n grid nodes. Although, using profile data ignores leveling problems, its principal pitfall lies on its true recognition of the 2D source structures [108]. Furthermore, since observational space is an integration of multidimensional responses, the output of the 2D approximations in solutions possessing greater level of scattering compared to the grid-based methods. TED technique possesses additional merits over the CED in its utilization of measured gradients rather than the computed gradients. This singular advantage recognizes the multidimensional technical responses, and the deconvolution procedures can be implemented without gridding the data. It's very inherent attribute of resampling of data onto profiles and grids is in essence an interpolation and functions as a low-pass filter for data that are prone to be more closely spaced than the node spacing. For this to be proven, CED and TED Programs are modified to conform to the irregularly spaced data representing ungridded data. However, adopting this form can lead to the formation of slower code when changing the position of the window within irregular data.

Application Euler deconvolution on simulation studies

Euler deconvolution can be applied on simulation studies using three models (point, prism and cylindrical mass models) purposely used to verify the Euler deconvolution methods and to demonstrate concepts that are related to gravity tensor gradients; these three models can be reviewed in the context of Euler deconvolution methods.

Point mass model (PoMM)

The potential for the point mass model is expressed in equation (5)

$$Ц = -\frac{GM}{r} \tag{5}$$

where

$$r = [(f - f_0)^2 + (g - g_0)^2 + (h - h_0)^2]^{\frac{1}{2}} \tag{6}$$

G is the gravitational constant; M is the mass and Ц is the disturbing potentials. If the first derivative is taken along the *f*–, *g*– and *h*– directions, equation (7), (8) and (9) are consequently produced

$$Ц_f = \frac{\partial Ц}{\partial f} = GM\frac{(f - f_0)}{r^3} \tag{7}$$

$$Ц_g = \frac{\partial Ц}{\partial g} = GM\frac{(g - g_0)}{r^3} \tag{8}$$

$$Ц_h = \frac{\partial Ц}{\partial h} = GM\frac{(h - h_0)}{r^3} \tag{9}$$

These formular for gravity anomaly are homogeneous of -2 degree. If the second derivatives of the disturbing potentials are taken along the *f*−, *g*− and *h*− directions, six of the nine second derivatives are produced as expressed in equation (10), (11), (12) (13), (14) and (15).

$$Ц_{ff} = \frac{\partial^2 Ц}{\partial f^2} = GM\frac{-3(f-f_0)^2+r^2}{r^5} \quad (10)$$

$$Ц_{fg} = \frac{\partial^2 Ц}{\partial fg} = GM\frac{-3(f-f_0)(g-g_0)}{r^5} \quad (11)$$

$$Ц_{fh} = \frac{\partial^2 Ц}{\partial fh} = GM\frac{-3(f-f_0)(h-h_0)}{r^5} \quad (12)$$

$$Ц_{gg} = \frac{\partial^2 Ц}{\partial g^2} = GM\frac{-3(g-g_0)^2+r^2}{r^5} \quad (13)$$

$$Ц_{gh} = \frac{\partial^2 Ц}{\partial gh} = GM\frac{-3(g-g_0)(h-h_0)}{r^5} \quad (14)$$

$$Ц_{hh} = \frac{\partial^2 Ц}{\partial h^2} = GM\frac{-3(h-h_0)^2+r^2}{r^5} \quad (15)$$

The remaining three other second derivatives can obtained using the symmetry features of the second derivative ($Ц_{fg} = Ц_{gf}$, $Ц_{fh} = Ц_{hf}$, $Ц_{gh} = Ц_{hg}$). All formulations are somewhat homogeneous of a degree of −3, with Ц satisfying the Lapalace equation as $Ц_{ff} + Ц_{gg} + Ц_{hh} = 0$ [102, 108].

The foretasted derivative relations between the disturbing potentials, gravity anomaly vector, and gravity tensor gradients result to varieties of distance weightings. These weight functions are representatives of inverse distance, inverse square distance and inverse cube distance respectively for the disturbing potential, the gravity anomaly and for tensor gradients which is much more conspicuous along the radial direction. In addition, the tensor gradient data with the accompanied rapid fall off extent with distance are less altered by possible interference from neighbouring geological structures than the other two [108, 138]. It also follows that gravity tensor gradients are more sensitive to shallower geological structures. The combination of the point model equations successively results in equation (16), (17), and (18).

$$(f-f_0)Ц_{ff} + (g-g_0)Ц_{fg} + (h-h_0)Ц_{fh} = GM\frac{-2(f-f_0)}{r^3} = -2Ц_f \quad (16)$$

$$(f-f_0)Ц_{gf} + (g-g_0)Ц_{gg} + (h-h_0)Ц_{gh} = GM\frac{-2(g-g_0)}{r^3} = -2Ц_g \quad (17)$$

$$(f-f_0)Ц_{hf} + (g-g_0)Ц_{hg} + (h-h_0)Ц_{hh} = GM\frac{-2(h-h_0)}{r^3} = -2Ц_h \quad (18)$$

This reveals that the model of the point mass appropriately fulfils the conditions of the Euler deconvolution methods for a structural index of two.

Prism mass model (PrMM)

Closed mathematical formulations for field potential anomaly have been systematically derived earlier by [139−140]. The formulae for potential field gradient were discovered in [141] Forsberg (1984). The lists of the formulae derived by [139] and [141] were compared by the formulae derived by [108] and further crosschecked with the Laplace equation and closed formulae for the horizontal components of the potential anomaly vector were consequently derived for this study.

In order to validate the Laplace equation derived for the prism mass model, the set of formulae of potential field and gradients for a prism model were defined by their respective co-ordinates x_1, x_2, y_1, y_2, z_1, and z_2 as displayed in Figure 2 and sequentially expressed in equation (19), (20), (21), (22), (23), (24), (25), (26), and (27).

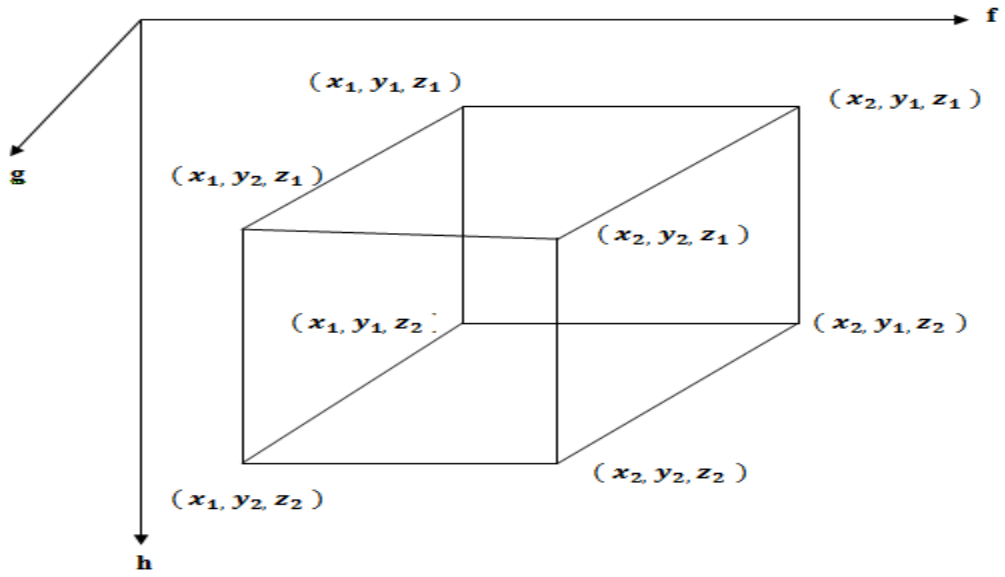

Figure 2: A prism mass model with respective coordinates [102]

$$\text{Ψ}_f = G\Delta\rho\left\{y\ln(z+r_1) + z\ln(y+r_1) - x\tan^{-1}\frac{yz}{x\,r_1}\right\} \times \begin{vmatrix} f & - & x_2 \\ f & - & x_1 \end{vmatrix}\begin{vmatrix} g & - & y_2 \\ g & - & y_1 \end{vmatrix}\begin{vmatrix} h & - & z_2 \\ h & - & z_1 \end{vmatrix} \quad (19)$$

$$\text{Ψ}_g = G\Delta\rho\left\{x\ln(z+r_1) + z\ln(x+r_1) - y\tan^{-1}\frac{xz}{y\,r_1}\right\} \times \begin{vmatrix} f & - & x_2 \\ f & - & x_1 \end{vmatrix}\begin{vmatrix} g & - & y_2 \\ g & - & y_1 \end{vmatrix}\begin{vmatrix} h & - & z_2 \\ h & - & z_1 \end{vmatrix} \quad (20)$$

$$\text{Ψ}_h = G\Delta\rho\left\{x\ln(z+r_1) + y\ln(x+r_1) - z\tan^{-1}\frac{xy}{z\,r_1}\right\} \times \begin{vmatrix} f & - & x_2 \\ f & - & x_1 \end{vmatrix}\begin{vmatrix} g & - & y_2 \\ g & - & y_1 \end{vmatrix}\begin{vmatrix} h & - & z_2 \\ h & - & z_1 \end{vmatrix} \quad (21)$$

$$\text{Ψ}_{ff} = -G\Delta\rho\tan^{-1}\frac{yz}{x\,r_1}\begin{vmatrix} f & - & x_2 \\ f & - & x_1 \end{vmatrix}\begin{vmatrix} g & - & y_2 \\ g & - & y_1 \end{vmatrix}\begin{vmatrix} h & - & z_2 \\ h & - & z_1 \end{vmatrix} \quad (22)$$

$$\text{Ψ}_{fg} = -G\Delta\rho\ln(z + r_1)\begin{vmatrix} f & - & x_2 \\ f & - & x_1 \end{vmatrix}\begin{vmatrix} g & - & y_2 \\ g & - & y_1 \end{vmatrix}\begin{vmatrix} h & - & z_2 \\ h & - & z_1 \end{vmatrix} \quad (23)$$

$$\text{Ψ}_{fz} = -G\Delta\rho\ln(y + r_1)\begin{vmatrix} f & - & x_2 \\ f & - & x_1 \end{vmatrix}\begin{vmatrix} g & - & y_2 \\ g & - & y_1 \end{vmatrix}\begin{vmatrix} h & - & z_2 \\ h & - & z_1 \end{vmatrix} \quad (24)$$

$$\text{Ψ}_{gg} = -G\Delta\rho\tan^{-1}\frac{xz}{y\,r_1}\begin{vmatrix} f & - & x_2 \\ f & - & x_1 \end{vmatrix}\begin{vmatrix} g & - & y_2 \\ g & - & y_1 \end{vmatrix}\begin{vmatrix} h & - & z_2 \\ h & - & z_1 \end{vmatrix} \quad (25)$$

$$\text{Ψ}_{gh} = -G\Delta\rho\ln(x + r_1)\begin{vmatrix} f & - & x_2 \\ f & - & x_1 \end{vmatrix}\begin{vmatrix} g & - & y_2 \\ g & - & y_1 \end{vmatrix}\begin{vmatrix} h & - & z_2 \\ h & - & z_1 \end{vmatrix} \quad (26)$$

$$\text{Ψ}_{hh} = -G\Delta\rho\tan^{-1}\frac{xy}{z\,r_1}\begin{vmatrix} f & - & x_2 \\ f & - & x_1 \end{vmatrix}\begin{vmatrix} g & - & y_2 \\ g & - & y_1 \end{vmatrix}\begin{vmatrix} h & - & z_2 \\ h & - & z_1 \end{vmatrix} \quad (27)$$

Where $r_1 = (x^2 + y^2 + z^2)^{\frac{1}{2}}$. $\Delta\rho$ is a mathematical symbol representing the density anomaly for the prism mass model. Laplace equation is further integrated to check the already derived formula.

$$Ш_{ff} + Ш_{gg} + Ш_{hh} = -G\Delta\rho \left[\tan^{-1}\frac{yz}{x\,r_1} + \tan^{-1}\frac{xz}{y\,r_1} + \tan^{-1}\frac{xy}{z\,r_1}\right] \begin{vmatrix} f & - & x_2 \\ f & - & x_1 \end{vmatrix} \begin{vmatrix} g & - & y_2 \\ g & - & y_1 \end{vmatrix} \begin{vmatrix} h & - & z_2 \\ h & - & z_1 \end{vmatrix} \quad (28)$$

$$Ш_{ff} + Ш_{gg} + Ш_{hh} = -G\Delta\rho \left[\tan^{-1}\frac{yz}{x\,r_1} + \tan^{-1}\frac{x\,r_1}{yz}\right] \times \begin{vmatrix} f & - & x_2 \\ f & - & x_1 \end{vmatrix} \begin{vmatrix} g & - & y_2 \\ g & - & y_1 \end{vmatrix} \begin{vmatrix} h & - & z_2 \\ h & - & z_1 \end{vmatrix} \quad (29)$$

$$Ш_{ff} + Ш_{gg} + Ш_{hh} = -G\Delta\rho \ \tan^{-1}\left[\frac{\frac{xz}{x\,r_1} + \frac{x\,r_1}{xz}}{1 - \frac{xz}{x\,r_1}\cdot\frac{x\,r_1}{xz}}\right] \times \begin{vmatrix} f & - & x_2 \\ f & - & x_1 \end{vmatrix} \begin{vmatrix} g & - & y_2 \\ g & - & y_1 \end{vmatrix} \begin{vmatrix} h & - & z_2 \\ h & - & z_1 \end{vmatrix} \quad (30)$$

$$Ш_{ff} + Ш_{gg} + Ш_{hh} = -G\Delta\rho \ \tan^{-1}[\infty] \times \begin{vmatrix} f & - & x_2 \\ f & - & x_1 \end{vmatrix} \begin{vmatrix} g & - & y_2 \\ g & - & y_1 \end{vmatrix} \begin{vmatrix} h & - & z_2 \\ h & - & z_1 \end{vmatrix} \quad (31)$$

$$Ш_{ff} + Ш_{gg} + Ш_{hh} = -G\Delta\rho \ \tan^{-1}\left[\frac{\pi}{2}\right] \times \begin{vmatrix} f & - & x_2 \\ f & - & x_1 \end{vmatrix} \begin{vmatrix} g & - & y_2 \\ g & - & y_1 \end{vmatrix} \begin{vmatrix} h & - & z_2 \\ h & - & z_1 \end{vmatrix} \quad (32)$$

$$Ш_{ff} + Ш_{gg} + Ш_{hh} = 0 \quad (33)$$

Two principal orientations are considered for the prism mass model. The first orientation possesses model sides that were parallel to the coordinate axes while the second orientation possesses model sides that were rotated through 45^0 about a vertical axis. The state of validition of Euler deconvolution for the prism mass model can be assessed by employing the analytical formulae $Ш_h$, $Ш_{hf}$, $Ш_{hg}$, and $Ш_{hh}$ without the integral limits by the relationship in equation (34).

$$Ш_{hf} + yШ_{hg} + zШ_{hh} = xG\Delta\rho \ \ln(y + r_1) + yG\Delta\rho \ \ln(x + r_1) - zG\Delta\rho \ \ln\frac{xy}{z\,r_1} = Ш_h \quad (34)$$

The structural index is equal to −1. This is evidently shown that the analytical formulation for the prism mass model excluding integral limits is homogeneous. However, the analytical formula of the prism mass model in line with the integral limits does not satisfy the homogeneity equation due to the fact that the prism mass model is a finite 3D source body and the contribution of the surrounding edges cannot be separated. This in turn leads to an effective structural index with accompanied varying distance, against an assumption within the theoretical provisions of Euler deconvolution with the attribute of constant SI due to a single simple source body [108, 143]. However, Euler deconvolution can still be applied to the prism mass model to obtain the required absolute Euler solutions [108].

Cylindrical mass model (CMM)

A cylindrical mass model has been thoroughly harnessed for the effective evaluation of the Euler deconvolution methods. Due to the absence of concrete closed formula readily available for the computation of the required potential field anomaly vector as well as the tensor gradients of the cylindrical mass model, the algorithm was consequently developed by [144] can therefore be applied. For the body to be modeled in this method, it is exemplified by a polyhedron comprising of triangular facets. After this approach, the anomaly can be transformed into two horizontal components of the anomaly vector using the empirical formula adopted by Vening-Meinez enshrined with Fast Fourier transform [108, 145]. On the basis of these three components, the convolution and deconvolution techniques described by [146] and [147] can be utilized in deriving

the six independent potential tensor gradient components thereby making the Euler deconvolution techniques to be successfully applied to a cylindrical mass model with potential field and gradients numerically estimated.

The Werner deconvolution technique is very resourceful and simple for preliminary interpretation of potential field data for isolated bodies [148−149]. Werner deconvolution technique operates on based on the assumption that the source is vertical thin dike, but it can be applied to other type of bodies with assumption that the body is made up of diverse thin dikes. The significance and profitability of the method is widened by the fact that the horizontal gradient of the total field induced by the edge of a thick interface body is equivalent to the total field from a thin dyke. This technique has been proven to be very much appreciable, as no initial model for the interpretation is required [149, 150−152]. [148] once presented a method of interpreting magnetic anomalies of two-dimensional sheet like causative bodies where the anomalies and the distances from the point of observation along the profile of investigation are arranged to form a linear equation with its coefficients related to the parameters of the sheet. The method is widely called Werner deconvolution technique. If this method is placed side by side in comparison with the conventional method like the curves that characterized the method, the expectation of Werner deconvolution method is to produce a better and more reliable result, since all the data in disposition on the profile are well utilized in the interpretation. If compared to the normal inversion method which gives recognition to the initial values of the parameters and iteratively improve them, we observe that Werner deconvolution is more accurate and less engaging because it does not require any initial values of the observed parameters to be fed or imputed to the computing system. Over the years there have been increasing tendencies on the application of Werner deconvolution method to the tracing of basement structures on the basis of surrounding clusters of fictitious positions of sheets [150−156]. [157] pointed that these aforementioned clusters are confined to contacts and faults in the basement on the conditions that they are widely separated and very steep but when moderately dipping, close, slightly shallow and smooth edge structures are encountered, the Werner's method does not make provision for any reliable interpretation. In essence, we can draw our inferences and attest that the method is simple in terms of approach, fast in terms of speed of accomplishment and proven to be reliable only when it is confined for the interpretation of the associated anomalies with simple isolated geometric bodies.

Although, the presentation of Werner deconvolution is with reference to the magnetic anomalies of sheets, yet, the method can be generally adapted to variety of geophysical models. According to [158], the observed anomalies or its horizontal derivative of a large set of field geophysical models can be re-organized to form a linear set of ordered equation of the type illustrated in equation (35).

$$h_0\,(F_{g,}\,U_g) = K_1\,h_1\,(F_{g,}\,U_g) + K_2\,h_2\,(F_{g,}\,U_g) + K_3\,h_3\,(F_{g,}\,U_g) + \ldots\ldots + K_n\,h_n\,(F_{g,}\,U_g) \quad (35)$$

where U_g represents the anomaly or its horizontal derivative, while F_g is a representation of the distance of the anomaly or the derivative measured from a fixed reference, $h_0\,(F_{g,}\,U_g)$, $h_1\,(F_{g,}\,U_g)$, ……$h_n\,(F_{g,}\,U_g)$, are the functions that are easily computed from $F_{g,}$ and U_g and K_1, K_2, $K_{3,}$ ……K_n are the unknown coefficients that are empirically linked with the model parameters. Linear equations corresponding to the above type can be transformed for each observation point while n normal equations are systematically derived and solved for the unknown coefficients. The coefficients, $K_1, K_2, K_{3,}$ ……K_n can be conclusively utilized to deduce the parameters of understudied model. The principal challenge with this method is that the linear equation generally possesses more coefficients than the observed parameters, with their

corresponding number increasing with the regional components of the anomaly present in the profile. Werner deconvolution method can be consequently modified by utilizing the positions of point pairs with equal anomaly values, instead of adopting varying individual points in the Werner deconvolution technique. Such a modification goes a long way in reducing the set of linear equations to a great extent. The modified method is therefore applied to both the synthetic and actual field data of a horizontal circular cylinder [159].

The generally adopted equation for the magnetic anomaly ΔH in any component either vertical, total or horizontal field along a profile of a horizontal circular cylinder is presented in equation (36) as provided by [160].

$$\Delta T = K \frac{[H^2 - (F - d)^2]\, L - 2M[(F - d)]\, H}{[(F - d)^2 + H^2]^2} \quad (36)$$

where *H* represents the depth to the centre of cylinder, *F* represents the interval or distance covered by the anomaly point P drawn from an arbitrary reference *R* in the profile, *d* is the lateral distance from the reference horizontally drawn from the reference to the position of the cylinder.

$$K = 2\pi R^2 S' \quad (37)$$

$$L = \sin \Phi' \text{ and } M = \cos \Phi' \quad (38)$$

where Φ' represents the dip of the effective magnetization and S' and Φ' in equation (37) and (38) respectively are the adopted generalized parameters connecting the magnitude of effective magnetization S, its dip Φ and direction D_m along which the anomalies are measured by the equations (39) and (40) respectively.

$$S' = S\ (1 - cos^2 \alpha\, cos^2 D_m)^{\frac{1}{2}} \quad (39)$$

$$\Phi' = \Phi - tan^{-1} \left(\frac{\sin \alpha}{tan\, D_m}\right) \quad (40)$$

The values of i, $\frac{\pi}{2}$, and 0 are captured by D_m to be taken for anomalies in the total field and its corresponding vertical and horizontal components respectively. α is the representation of the strike of the cylinder with positive measurement tilted towards the east from the magnetic north. Adapting an inversion scheme in an attempt to determine the values of d, H and Φ' setting aside the size parameter K. The subsequent cross multiplication and rearrangement of individual terms in equation 36 yields a linear equation of the form expressed in equation (41).

$$F^4\Delta T = K_1F^3\Delta T + K_2F^2\Delta T + K_3F\Delta T + K_4F^2\Delta T + K_5F\Delta T + K_6\Delta T + K_7. \quad (41)$$

where

$K_1 = 4d$

$K_2 = -(6d^2 + 2H^2)$,

$K_3 = 4d\,(d^2 + H^2)$,

$K_4 = -L$

$K_5 = 2\,(Ld - MH)$,

$K_6 = -(d^2 + H^2)^2$ *and*

$K_7 = -(LH^2 - Ld^2 + 2MdH)$

Equation (7) is a representation of the seventh order equation versus four unknown model parameters. However, two points can at least be located with which the anomaly values are equal on a profile. If F_1 and F_2 are the observed distances linked to the points of equal anomaly, ΔT =ΔT (F_1) = ΔT (F_2) as displayed in Figure 4. Independently, F_1 and F_2 are expected to satisfy equation (41). The expression of such equations and consequent subtraction of one equation from the other yields the output expressed in equation (42).

$$(F_2{}^2+F_1{}^2)(F_2+F_1)\,\Delta T = K_1(F_2{}^2+F_1{}^2+F_1F_2)\,\Delta T+K_2(F_2{}^2+F_1{}^2)\,\Delta T+K_3\Delta T+K_4(F_2+F_1)+K_5 \qquad (42)$$

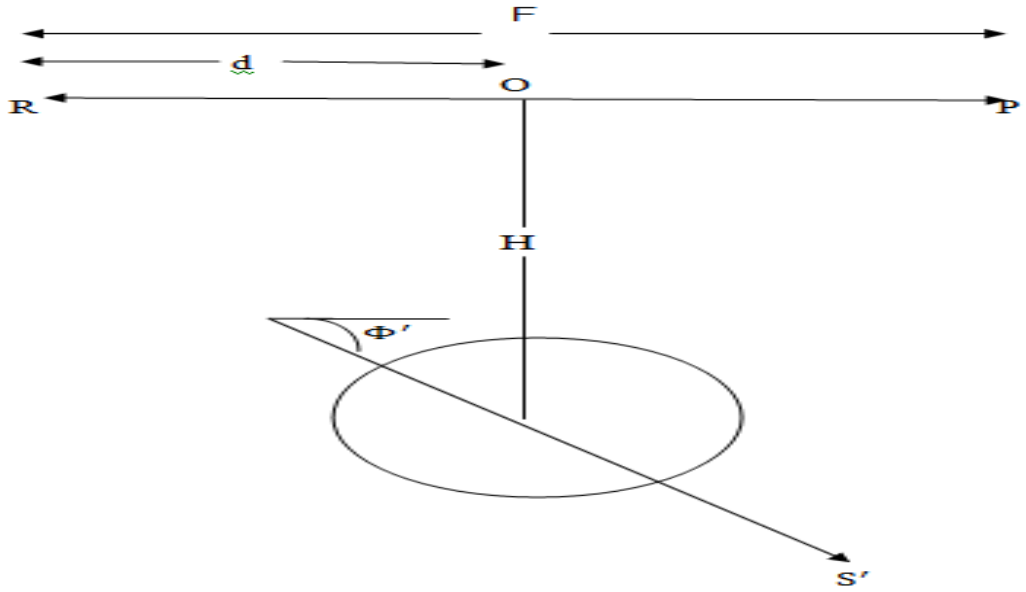

Figure 3: Geometric Parameters of the modeled Vertical Cylinder [102]

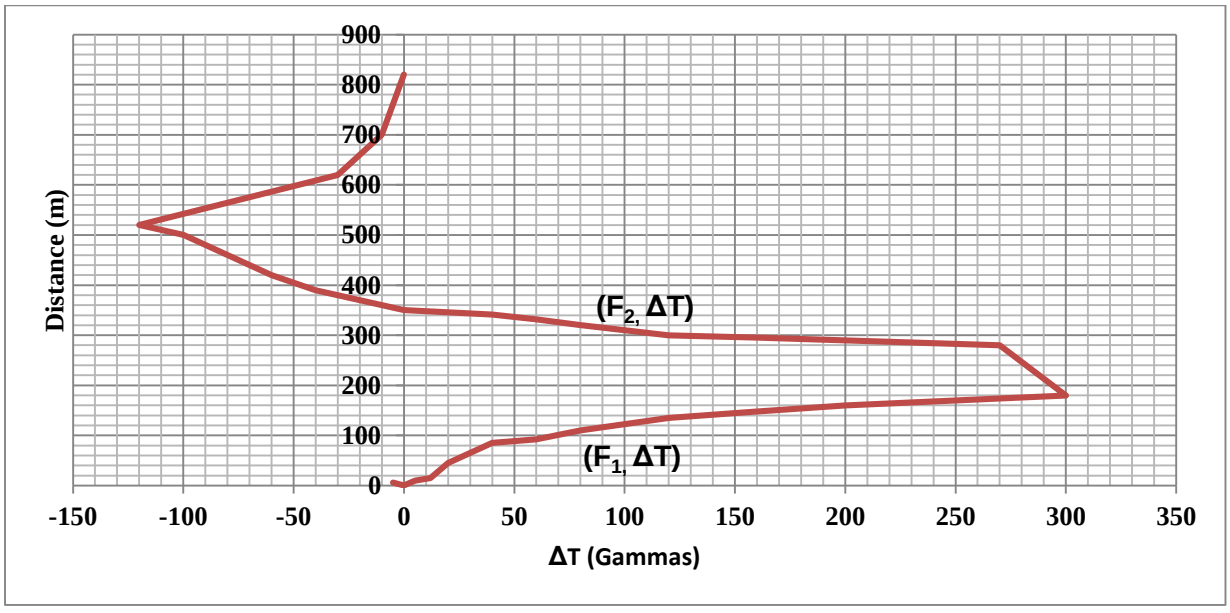

Figure 4: A modeled example of synthetic vertical magnetic anomaly profile over a horizontal cylinder [102, 108]

Equation 42 is a representation of fifth order equation for the four model parameters. This linear equation serves as a connector the calculable function $(F_2{}^2+F_1{}^2)\,(F_2+F_1)\,\Delta T$ to other calculable functions $(F_2{}^2+F_1{}^2+F_1F_2)\,\Delta T$, $(F_1+F_2)\,\Delta T$, ΔT and (F_2+F_1). Several sets of values of ΔT, F_1 and F_2 can be scaled from the field profile as displayed in Figure 4. Many linear equation of the form of equation (42) can be framed as the number of these sets with five constructed normal equations and their corresponding coefficients K_1 to K_5 are determined. These coefficients are then utilized to sequentially calculates the values of d, H and Φ'. The values of d and H are obtained from K_1 and K_2, while L and M are solved from K_4 and K_5, in successive pattern as shown equation 43 to 48.

$$d = 0.25K_1 \tag{43}$$

$$Z = [-0.5(K_2 + 6d^2)]^{\frac{1}{2}} \tag{44}$$

$$L = -K_4 \tag{45}$$

$$M = \frac{-0.5\,(K_5 + 0.5\,K_1\,K_4)}{H} \tag{46}$$

$$\Phi' = tan^{-1}\left(\frac{L}{M}\right) \tag{47}$$

$$K = [K_2 + M^2]^{\frac{1}{2}} \tag{48}$$

The method can therefore be programmed in order to determine the model parameters of the horizontal cylinder. Despite the possible minor errors that may ensue due to digitization procedures and measurement of distances, these techniques have proven to be satisfactory with the interpreted values matching closely with the synthetic data [161].

Data Acquisition and Processing.

The aeromagnetic datasets of Ado-Ekiti and its environs (sheet 244) that were acquired from the Nigerian Geological Survey Agency (NGSA) were prepared with Microsoft Excel program, and processed and interpreted using Oasis Montaj 8.4V. The datasets were imported and transferred to Universal Transverse Mercator (UTM) Zone 31N from UTM Zone 32N to sustain a constant coordinate system and avoid incoherence and misinterpretation of the acquired data by minimizing possible distortion over certain location in the study area as it is found within the UTM Zone 31N [162−163]. According to Nigerian Geological Survey Agency [164−165], the acquired datasets were part processed by Fugro Airborne Surveys (Leidschendam, Netherlands) using UTM of Zone 32N (UTM-32N) projection and World Geodetic System, 1984 (WGS84) as the reference datum. The WGS84 is a standard and established global datum utilized for determining varying position on the earth's surface. The WGSS84 is a reference system used by the satellite navigation system like GPS harnessed in diverse mapping applications. It is also utilized for determining positions on the earth's surface. The WGSS84 datum is defined and maintained by the United States National Geospatial-Intelligence Agency (NGA). Coordinates computed from GPS receivers are typically provided in terms of the WGS84 datum. WGS84 is compatible with the International Terrestrial Reference System (ITRS). De-culturing, tie-line and micro-leveling are some of the pre-processing operations carried out on the data. The datasets were given out by NGSA as an ASCII file comprising of X, Y and Z columns corresponding to the longitudes, latitudes and their matching total magnetic field intensities respectively. The total magnetic field intensity "Z" was stripped of 33,000nT for ease of processing the airborne data [164].

In this study, the Euler deconvolution algorithm provided by Geosoft Oasis Montaj ™ was used for source location and depth determination of causative magnetic bodies from gridded aeromagnetic data. The map thus produced from the processing reveals the locations and the

corresponding depth estimation of geologic sources from investigated profiles at estimated level of certainty. This is in line with works of [111]. Structural Index (SI) values 1.0 and 2.0 were used on the bases of available geological models of the source to be individual dykes, sills and horizontal cylinder as in this case of large plutons respectively [167]. The derived solutions were further polished by using the windowing technique in order to reduce uncertainty to the barest minimum. This was accomplished by considering the obtained Euler deconvolution solutions to accept maximum % depth tolerance of 10%, thus depth uncertainty (DZ in %) greater than 10% were rejected consequently. Similarly, Horizontal uncertainty (DX in %) was set to 20% which automatically opens mask to the outputs that fall out of the specified windows. Minimum window size was adopted since the maximum width of anomaly dependent on field observation around 250m [168]; this value ensures that a solution point constitutes a single anomaly point while the general solutions were obtained by plotting only solutions that are within acceptable limit in order further reduce possible spurious results.

RESULTS AND DISCUSSION

Total Magnetic Intensity Map of Ado- Ekiti

The total magnetic data was gridded with a 100m grid space to show the spatial distribution of negative anomaly. The amplitude of a magnetic anomaly is directly proportional to magnetization which depends on magnetic susceptibility of the rocks [1, 170]. The magnetic intensity level in the study area ranges from -977nT to 428nT. Which revealed the lithological variation of the subsurface of the study area classified as high and low amplitudes with patches of intermediate/moderate magnetic amplitude (Figure 5). Some negative magnetic values signifying prominent low amplitude magnetic anomalies ranges from -977nT to -1nT displayed in blue color in the Northern and southwest portion of the study area with further distribution in patches as a result of low magnetic rocks present in the study area namely un differentiated schists, quartz, porphyritic granite and migmatite gneiss that are noted for low magnetic signature [1, 170]. The regions of intermediate/moderate amplitude of magnetic anomaly range in values from 1 to 61are displayed in green and yellow colors. These were distributed across the study area which may be due to the presence of moderately high magnetic rocks (biotite-rich granite and migmatite-gneiss) formed under metamorphic condition. The total-field exhibiting high amplitude anomalies is associated with high intensities ranges from 68nT to 428 nT. Shown in red and pink colors were mostly observed in the central portion of the study area with patches in the NW and SW portions of the TMI map (Figure 5). These values identify charnockite, porphyritic granite as constituent rocks in Ijare, Ilara-Mokin and other settlements

Charnockites are a type of igneous rock that contains significant amounts of orthopyroxene which can be associated with increased magnetic susceptibility. Porphyritic Granite with its distinctive large feldspar phenocrysts can also exhibit varying magnetic intensities. The presence of magnetic minerals within the porphyritic granite such as magnetite or ilmenite can influence its magnetic properties. The magnetic intensity of these rocks is influenced by various factors such as the presence and abundance of magnetic minerals, the orientation and alignment of these minerals and the overall rock texture. Magnetic susceptibility is a measure of how easily a material can be magnetized, and it is often used to characterize the magnetic properties of rocks. Charnockites generally exhibit higher magnetic susceptibility values compared to some granites. While charnockites and porphyritic granites can have relatively high magnetic intensities, there can be variations with their rock types. The presence of fractures and other geological features can also affect the local magnetic intensity in the investigated area. The output of total magnetic image revealed the difference in locations of high and low magnetic intensities (Figure 5) with an

indication that the study area is a typical basement terrain, with location of high, intermediate and pocket of low magnetic susceptible bodies

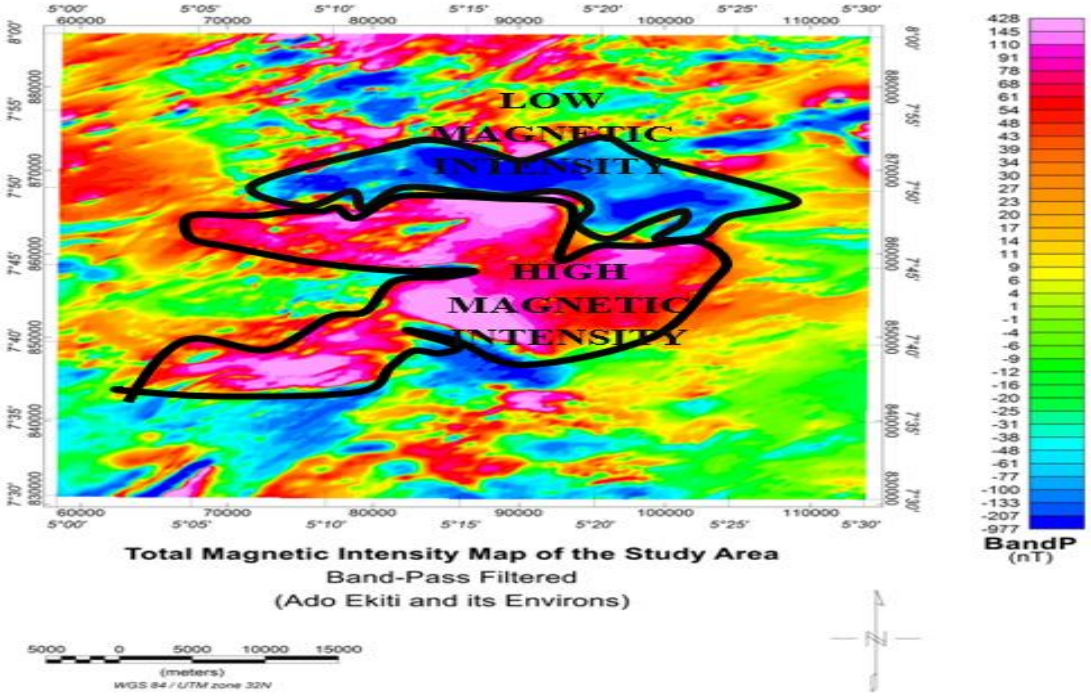

Figure 5: Total Magnetic Intensity (TMI) Map of Ado Ekiti and Adjoining Areas

Euler solution was integrated in the determination of the depth to the magnetic sources in the investigated area by setting up an appropriate structural index (SI) as displayed in Figure 6. The gridding intervals enable the recognition of any anomaly that is up to 75m wavelength. Therefore, many solution points with a sum of 34,595 were successfully obtained. Output with the tightest cluster winding around recognized sources is likely to grant the best solution and is consequently accepted. However, the obtained solution was windowed for the selection the most accurate output. These solutions were derived for varying SI values of 0, 1 and 2 with a mean error in depth estimation less than the required maximum tolerance of 11% while the window size of least unreal solutions was adopted. It was therefore observed that, for S.I equals to 1 (dike model) was the best fit (Figures 6). The solutions produced realistic outputs that were consistent with the geological model type of the study area. The solutions above the tolerance levels of the observed errors were rejected. Maximum depth limit was set for 250m, horizontal uncertainties that were found to be greater than 10% was rejected while the offset limit X and Y directions were likewise set to maximum of 5%. The windowed Euler deconvolution solution points were also found to coincide weakly with regions of heavy/high analytic signal amplitude and therefore serves as regions of representing meaningful anomalies and they are in dyke (Figure 7).

Table 1: Structural Index or Geologic Models [110, 169]

Geological models	**Number of infinite dimension**	**Gravity S.I**	**Magnetic S.I**
Sphere	0	2	3
Pipe	1 (Z)	1	2
Horizontal cylinder	1 (X and Y)	1	2

Dyke	2 (Z and X and Y)	0	1
Sill	2 (X and Y)	0	1
Contact	3 (X,Y and Z)	0	0

Euler depth gives a crtical but beneficial inforrmation about the topographic architecture of the basement complexes. The windowed Euler depth solutions are with color coded circle which also serves as an indication of depth ranges with the corresponding size defining the depth variation within the range limits. The typical characteristics of magnetic model type are show in table 2 while the Euler depths output are displayed in Table 3. Solutions revealed for Ado Ekiti reveals relatively deep basement source that were greater than 200m beneath mean sea level in depth observed at Ilawe Ekiti as it gets shallower both in the northwards and southwards direction. Euler depths output generally varied from 1m to 2223.9m overlapping with the rock contact in the study area but depths values found between 0 and 132m beneath sea level correspond to part of the study area where the basement rocks were overlain by clastic materials. Euler depth found below the datum were distributed over the investigated area and are less noticeable.

Table 2: Structural indices for simple models and their characteristic magnetic model types [166]

Structural Index	**Type of Magnetic Model**	**Typical Characteristic**
0.0	Contact with large extent	Interlocked Intertwined circles with no particular order
0.5	Contact with small extent	Interlocked/Intertwined circles in a linear pattern in rows
1.0	Sills and dyke, thin prism with large circles	Interlocked/intertwined circles in a straight line
2.0	Vertical and horizontal cylinder	Interlocked/intertwined circles with neatly with regular circumference and vertical pipe
3.0	Sphere	Sphere or spherical bodies of common circles connected to them

The integration of the windowed Euler solution map with the proposed geologic map reveaLs that these magnetic sources are in alignment with the observed lineaments that serve as host structures to these bodies of dykes. Settlements around the study area such as Iyin-Ekiti (600-1000m); Ilawe-Ekiti (1500-2200m) sections of Ogunru Forest Reserve (250-750m) Igbara Odo (0 to 100m and 0 to 1500m) are respective indications of negative and positive anomalies with Erijiyan (750-1500m) and Apata Hill (250-1000m), all correlation to section of the study area underlain by lineament and folds which serves as host of these magnetic sources. These settlements fall within the basement terrain with varying source depths solution ranging from approximately 100m to 2200m [170].

Table 3: Statistical Reports of Depths Estimation output from Euler-Deconvolution

Statistical	**Depths to magnetic Source (m)**
Minimum	132.2
Maximum	2233.9
Mean	213.6

Standard Deviation	142.7 3930483.8

Werner deconvolution is a technique that is utilized in aeromagnetic data processing and interpretation to estimate the parameters of magnetic sources (depth, width, and dip) from magnetic anomaly profiles. It is a type of deconvolution method used by fitting elementary models to segments of a magnetic anomaly profile. The Werner deconvolution equation is a set of linear equations derived from the magnetic field response of a model, and these equations are solved using the anomaly data to find the source parameters. It helps to extract information about the subsurface from the location and depth of magnetic sources from magnetic anomaly data collected during aeromagnetic surveys. It helps to interpret the shape and characteristics of magnetic anomalies by assuming that the anomalies are caused by simple geometric bodies (like thin sheets or horizontal cylinders) [171].

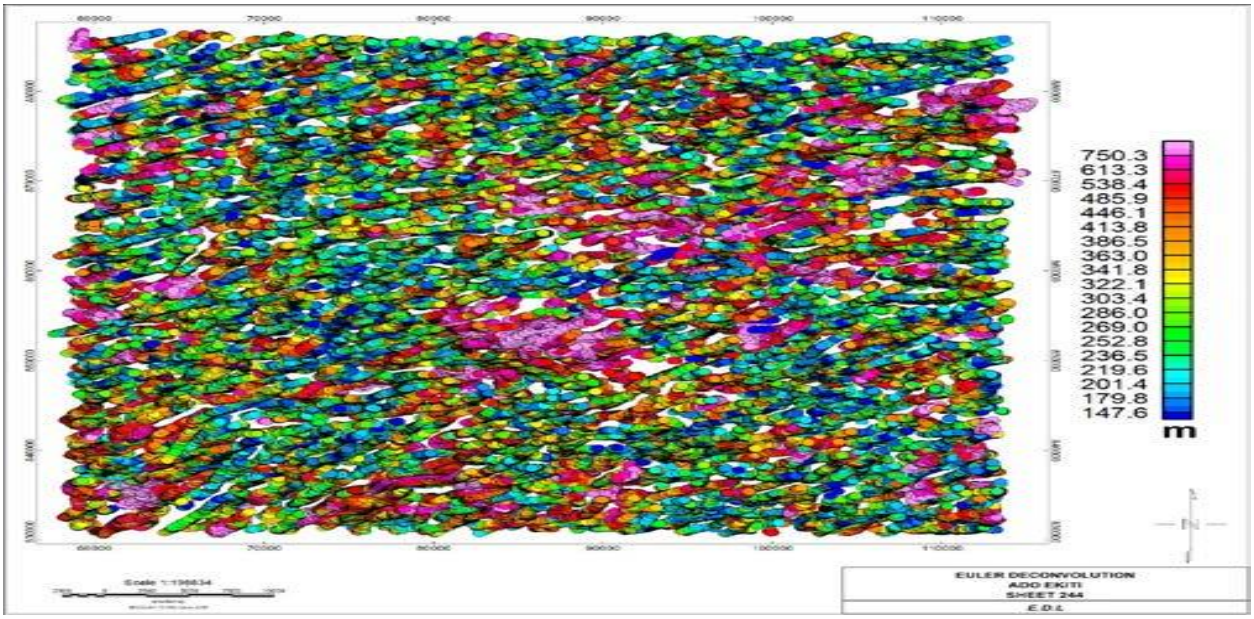

Figure 6: Standard Euler Solution Map of the Ekiti and its adjoining areas.

The core of Werner deconvolution involves formulating a set of linear equations based on the magnetic field response of a model (e.g., thin sheet) to the known magnetic field. These equations relate the observed magnetic anomaly values at different locations to the model parameters (like depth, location and dip). The equation is often expressed as a matrix equation, where the magnetic anomaly values are the measured and computed data as well as the model parameters are the unknowns to be determined.

Solving the Werner Deconvolution equation is achieved by using techniques or Singular Value Decomposition (SVD). These techniques find the best solution to the equation system minimizing the error between the calculated and observed magnetic anomaly values.

Werner deconvolution is widely used in geological and geophysical surveys to interpret aeromagnetic data. It can help to identify the presence of magnetic bodies, such as dikes, faults or ore deposits and estimate their depth and location. The results of Werner deconvolution can be

used to create models contour maps and understand the geological structure of the area. Limitations of Werner deconvolution are that it assumes that the magnetic anomalies are caused by simple geometric models which may not always be accurate. It can be challenging to interpret magnetic anomalies caused by Complex in multi-source equations; the accuracy of the results depends on the quality and resolution of the aeromagnetic data [149]. The Werner deconvolution method is more complex than the Euler method because it resolves the local regional and solve for two thin sheets or an interface within the same window. The basic formula for the magnetic field is defined by [148] as

$$T_n = \frac{(A_1 Z_1 + B_{M1}(x_o - x_1)}{(x-x_1)^2 + z_1^2} + \frac{(A_2 Z_2 + B_{M2}(x_1 - x_2)}{(x-x_2)^2 + z_2^2} + (Y_0 + Y_1 n + Y_2 n^2) \quad (49)$$

The first two bracketed terms in Werner's expression given in equation 49 are the magnetic field response for two thin sheets and the last given in brackets is a second order regional field contributions. Since, there is a need to solve for a single source magnetic anomaly with a linear regional, we can resolve to a simplified formula in equation (50)

$$T_n = \frac{(A_2 + B_M(n) + Y_0 + Y_1 n)}{(x^2 + z^2)} \quad (50)$$

where Y is the peak of MSS (Mineralized Source Strength) as the distance is set to zero. The last term represents the regional. The linear regional equation is employed for a number of locations and the matrix of the equations is solved for the source parameters while MSS peaks over the centre of magnetization and helps in the location of negative source. Figure 6 is a representation of Werner deconvolution function which utilized the horizontal and vertical derivatives in the computation of depth to basement of the anomalous magnetic bodies. The fundamental concept lies in the assumption that the magnetic source bodies are either dykes or contacts with infinite depth extent while applying a least-square approach to resolve for the location and position of the source body **[170]**. Two depth source models namely Dyke and contact models were assumed and their corresponding depths to basement were estimated using the Werner deconvolution function where he Dyke model fits the description of depth in the study area. Since Werner deconvolution transforms a complex magnetic anomaly into a linear set of equations to solve for these structural parameters, the resulting “curves” or “clouds” of points are interpreted to determine the depth of geological features of the study areas.

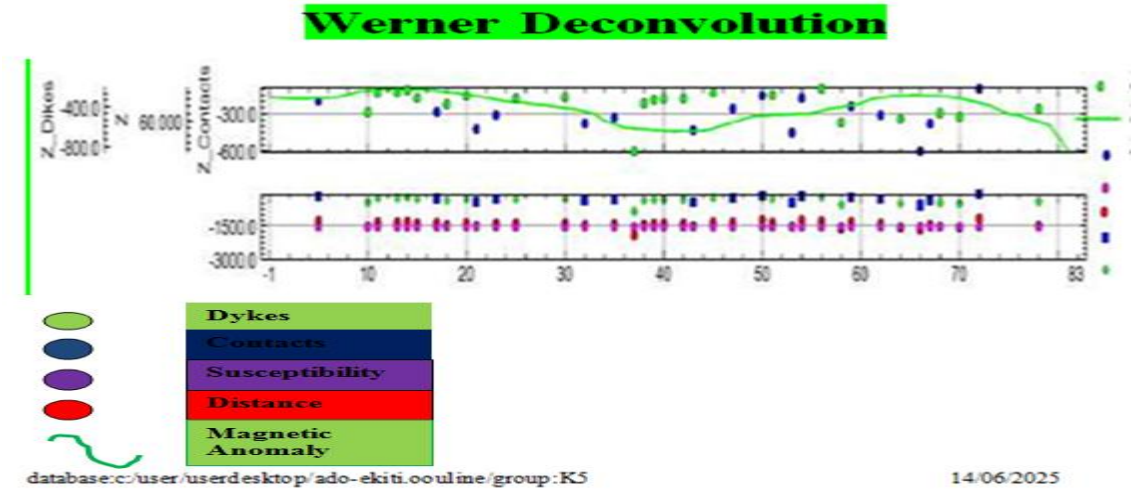

Figure 7: Wenner-Deconvolution function of Ado Ekiti and its adjoining areas

CONCLUSION

The study applied high-resolution aeromagnetic data to characterize the subsurface geology and delineate underlying structures of Ado-Ekiti and its environs in southwestern Nigeria. Detailed subsurface characterization and delineation of geological structures of the study and its environs is necessitated with the integration of Euler and Werner deconvolution techniques using the developed algorithms for tensor Euler deconvolution to regulate the profile, gridded and ungridded data. The techniques permitted the full potential gradient tensor and the components of vector to provide constraints on the Euler solution. The theoretical background governing the investigated profile as well as the adopted grid tensor Euler methods have been illustrated on isolated models namely point, prism, rotated prism, and cylindrical mass bodies. The collection, processing and enhancement of the aeromagnetic datasets over the area, led to proper mapping of the shallow subsurface geological structures and delineated the lithological variation. The magnetic image enhancement filter and other complementary fitting techniques were applied to enhance the dataset. Euler Deconvolution (ED) showed the minimum depth of 132.2m and maximum depth of 2233.9m for shallow and deep magnetic sources, Werner Deconvolution were used to confirm magnetic anomalies and delineated geological structures to be of intrusive contacts like dykes and sills. The output Euler deconvolution was associated with dykes on the other hand producing deeper depth range of 132.2 beneath mean sea level. While the contact model revealed shallow depth, the dyke model in the other hand revealed depth for the basement rock. The dike structure model therefore seemed to be of best fit for the study area because the occurrence of dyke model anomaly was positioned at a greater depth compared the contact model. The observed curve in Werner deconvolution plot represents the calculated clustered or best fit solution of anomalous geological bodies such as dikes or contacts along a geophysical profile of the magnetic survey in the study area (Figure 7). The curve or plotted points represents the source location and depth, geological structure interpretation, consistency clustering where the points in the plot that cluster together represent consistent, reliable solutions while scattered points indicate non-physical or noise-related solutions. This study has therefore proven that the integration of Euler and Werner deconvolution have proven to be valuable, semi-automated techniques in magnetics for mapping basement depth because they have enabled the rapid calculation of depth and location of subsurface structures without requiring complex initial 3D geological models with Euler being superior for spatial gridded mapping and Werner offering higher precision for or along 2D profiles; the subsurface structural geological characterizations, the consequent delineation/contact identification of most of the encountered structures in the area as well as the depth to basement estimation of the magnetic source bodies thereby serving as effective tool for the mapping of the basement architecture. In this study, Werner and Euler deconvolution It is therefore recommended that further analyses should be carried out in the study area since the plotted points might also indicate the dip angle and the magnetic susceptibility-thickness product of the source.

REFERENCES

[1] Telford, W. M., Geldart, I. P., and Sheriff, R. E. (1990). Applied Geophysics; 2nd Edn. 1006-10009.

[2] Nabighian, M.N., Grauch, V.J.S., Hansen, R.O., Lafehr, T.R., Li, Y., Pierce, J.W., Phillips, J.D and Rander, M.E. (2005). The historical development of the magnetic method in exploration geophysics. Geophysics; 70(6): 33-61. https://doi.org.10.1190/1.21337841

[3] Blakely, R.J. (1995). Potential theory in gravity and magnetic applications. Cambridge University Press. https://doi.org.10.1017/CNO9780511549816

[4] Ghosh, G.K., Gupta, R.D., Khanna, A.K., and Singh, S.N. (2012). Application of Euler

Deconvolution of Gravity and Magnetic Data for Basement Depth Estimation in Muzoram Area. Geohorizons; 1(3); 25-30.

[5] Adetona, A., Abbas, A and Mallam, A. (2013). Estimating the Thickness of Sedimentation within the Lower Benue Basin and Upper Anambra Basin Nigeria using both Spectra Depth Deformation and Source Parameter Imaging. ISRN International Journal of Geophysics; 20(3): 112-117. https://doi.org.10.1155/2013/24706

[6] Ndougsa-Mbarga, Yufenyiu, L.D., Quentin, Y.J and Tabod, C (2014). Delineation the Northern Limit of the Congo Craton Based on Spectral Analysis and 2.5D Modelling of Aeromagnetic Data in the Akonolinga-Mbama Area, Cameroon. Geofisica International; 53(1): 5-16.

[7] Bikoro-Bi-Alou, M., Ndougsa-Mbarga, T., and Tabod, C. (2014). Quantitative Interpretation of Magnetic Anomalies in Ebolowa-Djoum Area (Southern Cameroon). Geophysica; 50(1): 11-25.

[8] Ogunmola, J.K., Ayolabi, E.A., and Olobaniyi, S.B. (2016). Structural Depth Analysis of the Yola Arm of the Upper Benue Trough of Nigeria using High Resolution Aeromagnetic Data. Journal of African Earth Sciences. 124(1): 32-43. https://doi.org.10.1016/j.afrearsci.2016.09.008

[9] Njoku, I. (2016). Magnetic Basement Depth Re-evaluation over the Yola Arm of the Upper Benue Trough, Nigeria from 3D Euler Deconvolution and Spectra Inversion of High Resolution Aeromagnetic Data. International Journal of Scientific and Engineering Research; 7(4): 223-228.

[10] Ngoh, J.D., Ndougsa-Mbarga, T., Asembe, S.P., Meying, A., Owono-Amougwu, O.U.I and Tabod, C.T (2017). Evidence of Structural Facts Inferred from Aeromagnetic Data Analysis over the Guilder-Maroua Area, Northern Cameroon. Inter.Journal of Geosciences; 8(1): 781-800.

[11] Yandjimain, J., Ndougsa-Mbarga, T., Meying, T., Bi-Alou, M.B, Ngoumou, P.C., Asembe, S.P., Ngoh, J and Owono-Amougou, O.U.I. (2017). Combination of Tilt-Angle and Euler Deconvolution Approaches to Determine Structural Features from Aeromagnetic Data Modelling over Akonolinga-Loum Area (Centre-East, Cameroon). International Journal of Geosciences; 8(1): 925-947. https://doi.org.10.4236/ijg.2017.87053

[12] Mono, J., Ndougsa-Mbarga, T., Bi-Alou, M.B, Ngoh, J and Owono, Owono-Amougou, O.U.I. (2018). Inferring Subsurface Basement and the Contact Locations from Aeromagnetic Data over Loum-Minta Area (Centre-East Cameroon). International Journal of Geosciences; 9(1): 435-459. https://doi.org.10.4236/ijg.2018.97028

[13] Nwankwo, L.I and Abayomi, J.S. (2017). Regional Estimation of Curie-point Depths and Succeeding Geothermal Parameters from Recently Acquired High Resolution Aeromagnetic Data of the Entire Bida Basin, North-Central Nigeria. Geothermal Energy Science; 5(1): 1-9.

[14] Azab, A.A., Ramadan, M.A., and El-Sawy, M.I. (2019). An integrated Analysis of Gravity and Well Data for Deep-seated Structural Interpretation: a case study from Ras-Budran Oil field, Gulf of Suez, Egypt. Journal of Petroleum Exploration and Production Technology; 9(1): 177-189.

[15] Ayomide, A., Felix., O.O., Adeboye, M.B. (2025). Deformation of Depth to Magnetic Sources from Aeromagnetic Data of Idah, Kogi State using Eulr Deconvolution Technique. International Journal of Earth Sciences, Knowledge and Applications; 7(2): 18-21.

[16] Ukwuteyinor, U. B., Onwuemesi, A. G., Obiadi, I. I., Irumhe, E. P. and Osaghae, S.O. (2021). Estimation of depth to basement, heat flow and hydrocarbon potentials from

analysis of aeromagnetic data in some parts of bida basin. Journal of Basic Physical Research 10 (1), January 2021

[17] Njoku, J. O., Nwankwo, L. I., and Uche, E. I. (2022). Aeromagnetic evaluation of crustal structures in north-central Nigeria. International Journal of Earth Sciences; 76(4): pp. 210-225.

[18] Opara, A.I., Emberga, T., Oparaku, O., Essien, A.G., Onyewuchi, R.A., Echetama, H.N., Muze, N.E., and Onwe, R.M. (2015). Magnetic Basement depth Re-evaluation of Naraguta and Environs, North-central Nigeria using 3D Euler Deconvolution. Exploration and Mining Journal. 3(32): 29-42. https://doi.org.10.12691/ajmm-3-2-1

[19] Jekeli, C. (1985). On optimal Estimation of Gravity from Gravity Gradients at Aircraft Altitude. Revolution Geophysics; 23:301-311

[20] Askaris, A. (2014). Edge Detection of Gravity Sources via the Tilt Angle Total Horizontal Derivative of the Tilt Angle and New Normalized Total horizontal Derivative. Scholars Journal of Engineering and Technology; 2(1): 842-846.

[21] Zhou, W., Li, J., and Du, X. (2014). Semi-automatic Interpretation of Microgravity Data from the Subsurface Cavities using Curvature Gradient Tensor Matrix. Near Surface Geophysics; 125(5): 579-586. https://doi.org.10.10.3997/1873-0604.2014021

[22] Arisoy, M.O and Dikmen, V. (2015). Edge Enhancement of Magnetic Data using Fractional –Order Derivative Filters. Geophysics; 80(1): 7-13.

[23] Jayeoba, A and Odumade, D. (2015). Geological and Structural Interpretation of Ado-Ekiti Southwest and its Adjoining Areas using Aeromagnetic Data. Search and Discovery Article #30407 Extended Abstract from AAPG/SEG/SEPM Joint Technical Conference, Oxnard California. pp. 2-11.

[24] Howari, F.M., Aldouri, R and Sadiq, A. (2016). Gravity Investigations of Recent Sinkholes and Karst Pits of Dahal Al-Haman, State of Qatar. Environmental Earth Science. 75(5): 440. https://doi.org.10.1007/su2665-016-5298-x

[25] Abdelghany, O., Saima, M.A., Arman, H., and Fouler, A.R. (2017). Engineering Evaluation of Macrostructures in the Carbonate Rocks in Al-Ain Area, United Arab Emirates. International Conference on Engineering Geophysics, Al-Ain, Al-Ain, United Arab Emirates. 9th-12th October, 2017. https://doi.org.10.1190/iceg2017.078

[26] Murad, A and Gabir, A. (2017). Groundwater level Monitoring of the Quarternary Aquifer at Al-Ain City, United Arab Emirates using Geophysical Methods: In WSTA 12th Gulf Water Conference 28th to 30th March, 2017. Kingdom of Bahran Water in the GCC towards Integrated Strategies 70.

[27] Aboud, E., El-Masry, N and Ahmed, S. (2018). Microgravity Mapping for King AbdulAziz University Campus: Imaging Subsurace. Arabian Journal of Geoscience. 11(2): 691. https://doi.org.10.1007/s12517-018-4029-x

[28] Saibi, H., Hag, D.B., Alamri, M.S.M and Ali, H.A. (2021). Subsurface Structure Investigation of the United Arab Emirates using Gravity Data. Open Geoscience. 13(1): 262-271. https://doi.org.10.1515/geo-2020-0233

[29] Zhang, M., Qiao, J., Zhao, G and Lan, X. (2019). Regional Gravity Survey and Application in Oil and Gas Exploration in China. China Geology. 2(3): 380-388. https://doi.org.10.31035/cg2018108

[30] Okpoli, C.C and Akingboye, A.S. (2019). Application of High Resolution Aerogravity Data for Litho-structural and depth Characterization around Lgabi Area, Northwestern Nigeria. NRIAG Journal of Astronomy and Geophysics. 8(1): 231-241. https://doi.org.10.1080/20909977.2019.1689629

[31] Pham, L.T., Oksum, E., and Do, T.D. (2019). Edge Enhancement of Potential Field Data using logistic Function and Total Horizontal Gradient. Acta Geodynamics and Geophysics; 54(1): 143-155.

[32] Low, U., Absar, A., Duraiswami, R and Singh, A. (2020). Geophysical Exploration of Tura-Rajwadi Group of Hot Springs, West Coast Geothermal Province, Maharashtra, India and its Implications. Geothermics; 88(1): 652-665. https://doi.org.10.1016/j.geothermics.2020.101874

[33] Pham, L.T., Eldosouky, A.M., Oksum, E., and Saada, S. (2020). A new High Resolution Filter for Source Edge Detection of Potential Field Data. GeoCarto International; 37(1): 3051-3068. https://doi.org.10.1080/10106049.2020.1849414

[34] Mohammed, E.A., Pham, L.T., Mohammed, H., Pradhan, B.A. (2020). Comparative Study of THG, AS, TA, Theta, TDX and LTHG Techniques for Improving Source Boundaries Detection of Magnetic Data using Synthetic Models: A case study of from G-Um-mmquil North Eastern Desert Egypt. Journal of African Earth Science; 170(1): 521-532. https://doi.org.10.1016/j.jafrearsssci.2020.103940

[35] Jacob, T., Pannet, P., Beaubois, F., Baltassant, J.M., and Hannion, Y. (2021). Cavity Detection using Microgravity in a highly Urbanized Setting: A case study from reins, France. Journal of Applied Geophysics; 179(1): 673-678. https://doi.org.10.1016/j.jappgeo.2020.140113

[36] Melouah, O and Pham, L.T. (2021). An Improved ILTHG Method for Edge Enhancement of Geological Structures. Application to Gravity Data from the Qued Righ Valley. Journal of African Earth Sciences; 177(1): 6521-6534.

[37] Porzucek, S and Loj, M. (2021a). Depth Estimation Problems in Microgravity Survey. Acta Geophysic;. 69(1): 665-672. https://doi.org.10.1007/s11600-021-00553-1

[38] Mulugeta et al., 2021; Mulugeta, B.D., Fujimitsu, Y., Nishijima, J and Saibi, H. (2021). Interpretation of Gravity Data to Delineate the Subsurface Structures and reservoir Geometry of the Aluto-Langano Geothermal Field, Ethiopia. Geothermics; 94(1): 453-464. https://doi.org.10.1016/j.geothermics.2021.102093

[39] Eldosouky, A.M., Pham, L.T., Henash, A. (2022). High Precision Structural Mapping using Edge Filters of Potential Field and Remote Sensing Data: A case Study from Wadi-Umon Ghalqa Area, South Eastern Desert, Egypt. The Egyptian Journal of Remote Sensing and Space Science; 25(2): 501-503. https://doi.org.10.1016/j.ejrs.2022.03.001

[40] Prasad, K.N.D., Pham, L.T., and Singh, A.P. (2022a). Structural Mapping of Potential Field Sources using BHG Filter. Geocarto International; 37(26): 11253-11280.

[41] Prasad, K.N.D., Pham, L.T., and Singh, A.P. (2022b). A novel filter ImTAHG for the Edge Detection and a case study from Cambay Rift Basin, India. Pure and Applied Geophysics; 179(6): 2351-2364.

[42] Pham, L.T., Oksum, E., Kafadar, O., Trinh, D.T., Nguyen, D.V., Vo, Q.T., and Do, T.D. (2022a). Determination of Subsurface Lineaments in the Hoang Sa Islands using Enhanced Methods of Gravity Total Horizontal Gradient. Vietnam Journal of Earth Sciences; 44(3): 395-409.

[43] Pham, L.T., Nguyen, T.U.Y., Xuan, E.W., Eldosouky, A.M., Do, T.D., and Nguyen, T.Q. (2022b). The Utility of the Enhancement Techniques for Mapping Subsurface Structures from Gravity Data. Frontier Science Research Technology; 3(1): 11-19.

[44] Anthony, E.A., Likkasson, O.K., Maigari, A.S., Ali, S and Abubakar, A. (2023). Subsurface Structural Characterization as deduced from High Resolution Aeromagnetic Data over the Confluence Zones in Central Nigeria. Indonesian Journal of Earth Sciences; 3(1): 322-343. https://doi.org.10.52562/injoes.2023.600

[45] Teknik, V and Ghods, A (2017). Depth of magnetic basement in Iran based on fractal spectral analysis of aeromagnetic data Geophys. J. Int. (2017) 209, 1878–1891

[46] Pham, L.T. (2023). A Novel Approach for Enhancing Potential Fields: Application To Aeromagnetic Data of the Tuangiao, Vietnam. Europ Physical and Journal Plus; 138(12): 1-11.

[47] Folorunsho, I., Magaji, Y., Ajadi, J., Issa, U. (2024). Application of Euler and Werner Deconvolution Techniques in Delineating Tin Deposit in Okeso Area, Southwestern Nigeria. Proceedings of the Nigerian Society of Physical Sciences; pp. 10-13. https://doi.org.10.61298/pnspsc.20241.96

[48] Pham, L.T., Kemgang-Ghomsi, F.G., Eldosouky, A.M. (2025). Identification of the Structural Configuration of the Equitorial Atlantic Ridge from Satellite-derived Gravity Data using the Enhancement Techniques. Advances in Space Research; 75(2): 8425-8438. https://doi.org.10.1016/j.asr.2025.03.066

[49] Kwega-Ghomsi, S.L., Bisso, D., Ganno, S., Pham, L.T., Tenzer, R., Kwega-Ghomsi, F.E. (2025). Reassessing Tectono-structural units and Crustal Thickness Variations in South-West Cameroon using Satellite Gravity and Seismic Data. Journal of African Earth Sciences; 229(1): 132-142. https://doi.org.10.1016/j.afrearsci.2025.105698

[50] Ismail, F.F. and Saibi, H. (2025). A microgravity Investigation of the subsurface at the United Arab Emirates University Campus. Scientific Reports; 15(1): 225-232.

[51] Ghosh, G.K. (2022b). Delineation of Major Subsurface Structural Features and Source Depth Locations using 3D Euler Deconvolution Gravity Data at Northeastern Part of India. Acta Geophysica; 70(1): 2033-2044. https://doi.org.10.1007/s11600-022-00829-0

[52] Lasheen, E.S.R., Hassan, W., Eric, A., Azer, M.K. (2020). Implementation of Petrographical and Aeromagnetic Data to Determine Depth and Structural Trend of Homrit Waggart Area, Central Eastern Desert, Egypt. Applied Sciences; 12(17): 8782-8794. https://doi.org.10.3390/app12178782

[53] Ayomide, A., Felix., O.O., Adeboye, M.B. (2025). Deformation of Depth to Magnetic Sources from Aeromagnetic Data of Idah, Kogi State using Eulr Deconvolution Technique. International Journal of Earth Sciences, Knowledge and Applications; 7(2): pp. 18

[54] Raouf, A., Yue, J., Njeudjang, K., Tamehe, L.S., Onibudo, O.O. (2023). Remote Sensing and Geophysical Methods for Delineating Groundwater Resources in Schists hard rocks of the Adamawa Yade Domain, Cameroon. The Egyptian Journal of Remote Sensing and Space Science; 26(1): 217-230. https://doi.org.10.1016/j.ejrs.2023.02.006

[55] Owona-Nanji, W.G., Meying, S., Nyouma, R.N., Edjo-Minko, R., Foudikou, O and Bessong, M. (2025). Combined analysis of Magnetic Investigations and Geological Mapping of Babouri-Figuil Basin (Northern Cameroon): Implications for Hydrocarbon Prospects. Geosystems and Geoenvironment; 5(1): 5561-5573. https://doi.org.10.1016/j.geogeo.2025.100437

[56] Nekuye-Muafo, C.A., Basseka, C.A., Boum-Nkot, S.N., Som-Mbang, C.M., Njifeu-Tchoukewu, C.D., Kengne, Y.S., Tsopkeng, P.B., and Elame, J. (2018). Lineament Mapping in the Edea Area (Littoral Cameroon) using Remote Sensing and Gravimetric Data: Hydrogeological Implications. Journal of Applied Remote Sensing. 18(3): 2334-2348. https://doi.org.10.1117/1.jrs.18.032402

[57] Kobe, E.B., Franck-Marcel, A.M., and Arsene, M. (2025). ResUMES++: Resistivity Uncertainty Modelling for Environmental Study. Journal of Applied Geophysics. 241 (1): 3342-3356. https://doi.org.10.1016/jappgeo.2025.105797

[58] Opara, A.I., Emberga, T., Oparaku, O., Essien, A.G., Onyewuchi, R.A., Echetama, H.N., Muze, N.E., and Onwe, R.M. (2015). Magnetic Basement depth Re-evaluation of Naraguta

and Environs, North-central Nigeria using 3D Euler Deconvolution. Exploration and Mining Journal. 3(32): 29-42. https://doi.org.10.12691/ajmm-3-2-1

[59] Demirel, S., Alpar, B., Yalturak, C., Vardar, D., Kurt, H. (2020). Northern Segment of the North Anatolian Fault in the Gulf of Izmit Inferred from Marine Magnetic Anomalies. Marine Geophysical Research. 41(1):1-10.https://doi.org.10.10007/s11001-020-09399-6

[60] Aktas, G., Hisarh, Z.M., and Demirel, A.S. (2021). High Resolution Total Field Magnetic Anomaly Maps of Lake Iznik North-West Turkey: Assessment of Faults which play Important Roles in Tectonics of Lake. Geophysical Research. 42(3): 1-17. https://doi.org.10.1007/s11001-021-09442-0

[61] Hayatudeen, M., Bassey, N.E., Razaq, B. (2021). 2-D Modelling of High Resolution Aeromagnetic Data over Yola Arm of the Upper Benue Trough in Northern Nigeria. Global Journal of Pure and Applied Sciences. 27(2): 133-143. https://doi.org.10.4314/gjpas.v27i2.6

[62] Vardar, D., Alp, H., Demrel, S., Aykurt, A., Vardat, H and Alpar, B. (2021). Offshore/Onshore Correlation of the North-Anatolian Fault Deformatons in the Wasuum Sea of M armara National Hazard. 107(2): 1905-1923. https://doi.org.10.1007/s11069-021-04664-2

[63] Aktas, G., Hisarh, Z.M., and Demirel, A.S. (2022). Interpretation of the Tectonic Structure of Gemlik Bay using Magnetic Data. Tectonophysics. 863(1): 2231-2247.

[64] Kiyak, A., Pamuk, E., Koksal, S., Bakar, M.L., Tosuner, S. (2022). New High Resolution Aeromagnetic Anomaly Map of Turkiye and its various Derivative-Based Maps. Turkish Journal of Earth Sciences. 32(2); 231-247. https://doi.org.10.55730/1300-0985.1840

[65] Tarlowski, C., Gunn, P. J., & Mackey, T. (1997). Enhancements of the magnetic map of Australia. AGSO Journal of Australian Geology & Geophysics, 17(2), 77-82.

[66] Agoha, C.C., Onwubuariri, C.N., Mgbeojedo, T.I., Amasike, C.U., Agbakwuru, C.B., Njoku, J.O., Akaolisa, C.C.Z., Alexander, O.I., Ofoh, I. (2023). Aeromagnetic Data Integration and Source Body Evaluation using Standard Euler deconvolution Technique in Obudu Area, Southeastern Nigeria. Petroleum and Coal; 65(4): 1033-1041.

[67] Aktas, G. (2024). Edge Detection and Depth Estimation of Lake Sapanca, Eastern Marmara Region from High-Resolution Magnetic Data. Acta Geophysica (Applied Geophysics); 72(1): 3337-3354. https://doi.org.10.1007/s11600-023-01277-0

[68] Opara, A.I., Emberga, T., Oparaku, O., Essien, A.G., Onyewuchi, R.A., Echetama, H.N., Muze, N.E., and Onwe, R.M. (2015). Magnetic Basement depth Re-evaluation of Naraguta and Environs, North-central Nigeria using 3D Euler Deconvolution. Exploration and Mining Journal; 3(32): 29-42. https://doi.org.10.12691/ajmm-3-2-1

[69] Saleh et al. (2018). Azaiez, H., Gabtni, H., Bédir, M., and Campbell, S. (2018). Aeromagnetic study of buried basement structures and lineaments of the Sahel region (Eastern Tunisia, North Africa). Arabian Journal of Geosciences, 11, 140.

[70] Roy, L., Chouteau, M., & Keating, P. (2000). Depth estimation of magnetic sources by an improved Euler deconvolution method. Journal of Applied Geophysics; 44(2-3), 183-199.

[71] Phillips, C. V. Reeves, C. V. and Milligan, P. R. (2007). Aeromagnetic Surveys: Principle, Practice, and Interpretation. Geosoft ePublication; pp. 2321-2325

[72] Kaukau, B., Greillingb, R.O., and Mzenti,. J.P. (2001). Pan-African Strike-Slip Tectonics in Eastern Cameroon Magnetic Fabrics (AMS) and Structure in the Lom Basin and its Gniessic Basement. Precambrian Research; 174(1): 258-272. https://doi.org.10.1016/j.precamres. 2009.08.001

[73] Kwekam, M., Liegeois, J.P., Njonfang, E., Affaton, P., Hartmann, G and Tohoua, F. (2010). Nature, Origin, and Significance of Formopoea Pan-African High Calcium

Alkaline Plutonic Complex in the Central African Fold Belt (Cameroon). Journal of African Earth Sciences; 57(1): 79-95. https://doi.org.10.1016/j.jafrearsci. 2009.07.012

[74] Owona et al., 2011). Owona, S., Schulz, B., Patschbacher, L., Mvondo-Ondoa, J., Ekodeck, G.E., Tohoua, M.F., and Affaton, P. (2011). Pan-African Metamorphic Evolution in the Southern Yaounde Group (Oubanguide Complex, Cameroon) as revealed by EMD-Monazie Dating and Thermobarometry of Garnet Meta-pelites. Journal of African Earth Sciences; 59(1): 125-139. https://doi.org.10.1016/j.jafrearsci.2010.09.003

[75] Florio, G and Fedi, M. (2013). Multiridge Euler Deconvolution. Geophysical Prospecting. 62(2): 148-163. https://doi.org.10.1111/1365-2478.12078

[76] Porzucek, S and Loj, M. (2021). Microgravity Survey to Direct Voids and Loosening Zones in the Vicinity of the Mine Shaft. Energies; 14(1): 3021. https://doi.org.10.3390/en14113021

[77] Olatunji, S and Adebisi, W. (2022). Werner Deconvolution Techniques for the Interpretation of Residual Aeromagnetic Anomalies of Igbeti Schist Belt: Implication for Marble Exploration. Indonesian Journal of Geosciences; 9(2): 209-217. https://doi.org.10.17014/ijog.9.2.209-217

[78] Okwesili N.A, John, A.Y and Ossai N.M. (2025). Estimating the depth of basement rocks within the Guzabure and Gudumbali area of the Nigerian sector of the Chad basin using a spectral analysis technique. International Journal of Physical Sciences. 20(1): pp. 26-39.

[79] Uieda, L., Souza-Junior, G.F., Uppal, I., Oliviera-Junior, V.C. (2025). Locating Sources of Potential Data through Inversion of Euler's Inhomogeneity Equation. Earth-Arxiv, Geophysical Journal International; 241(3): 1536-1552.

[80] Melo, F.F., Barbosa, V.C.F., Uieda, L., Oliviera, V.C., Silver, J.B.C. (2013). Estimating the Nature and the Horizontal and Vertical Positions of the 3D Magnetic Sources using Euler Deconvolution. Geophysics. 78(6): 187-198. https://doi.org.10.1190/geo2012-0515.1

[81] Reid, A.B., and Thurston, J.B. (2014). The Structural Index is Gravity and Magnetic Interpretation: Errors, uses, and Abuses. Geophysics; 79(4): 161-166

[82] Robinson, R.A.J., Brezina, C.A., Parish, R.R., Horstwood, M.S.A., Oo, N.W., Bird, M.I., Thein, M., Waters, A.S., Oliver, G.J.H., Zaro, K. (2014). Large Rivers and Origins: The Evolution of the Yarlung Tsangpo-Irrawaddy System and the Eastern Himalayas Syntaxis. Gondwana Research. 26(1): 2112-2121. https://doi.org.10.1016/j.qr2013.07.002

[83] Ghosh, G.K. (2015). Interpretation of Gravity Anomaly and Crustal Thickness Mapping of Narmada-Sum Lineament in Central India. Journal of Geological Society of India; 86(3): 263-274. https://doi.org.10.1007/s12594-014-0077-3

[84] Ghosh, G.K. (2016). Automatic Delineation of Structural Boundaries using Curvature Analysis of Bouguer Gravity Data in Parts of Northwest Himalaya. Journal of Geological Society of India; 91(5): 589-595. https://doi.org.10.1007/s12594-018-0909-7

[85] Ghosh, G.K. (2019). Interpretation of Gravity Anomaly to Delineate Thrust Fault Locations at the Northeastern Part of India and its Adjacent Areas using Edge Detection Technique, Tilt Derivative and Cosθ Analysis. Acta Geophysica; 67(1): 1277-1295. https://doi.org.10.1007/s11600-019-00345-8

[86] Ogbudu, P. A. Okon, E. E. Ugar, S. I. Lebo, S. E. Alo, G. A. and Okereke, C. S. (2025). Sediment thickness distribution and 2D depth model of the Ikom Basin, southeastern Nigeria, using high-resolution aeromagnetic data. Global Journal of Pure and Applied Sciences; 31(2): 211-227..

[87] Mikołajczak M., Barmuta J., Ponikowska M., Mazur S. and Starzec K. (2021). Depth-to-basement study for the western Polish Outer Carpathians from three-dimensional joint inversion of gravity and magnetic data. Journal of Geosciences; 66 (1):15–36

[88] Ndougsa-Mbarga, T., Feumo, N. S. A., Manguelle-Dicoum, E., & Fairhead, D. J. (2012). Aeromagnetic Data Interpretation to Locate Buried Faults in South-East Cameroon. Geophysica; 48(1-2), 49-63.

[89] Liozibhie, A.J., Ejepu, J.J., Szafarczyk, A., Agbasi, O.E., Inyang, N., and Egu, O.I. (2023). Retrospective Appurtenance of Euler and Werner Deconvolution Contiguity for Source Depth Excogitation of Bouguer Anomalies in Benue Trough, Nigeria. Journal of Sedimentary Environment; 8(3): 889-915. https://doi.org.10.1007/s43217-023-00146-7

[90] Kominis, I. K., Kornack, T. W., Allred, J. C., and Romalis, M. V (2003). A subfemtotesla multichannel atomic magnetometer, Nature, Volume: 422, Issue 6932 Pages 596-599

[91] Faruwa, A. R. Qian, W., Obafunmilayo, O. S. Daramola, B. B. Ali, M. A. H. Dusabemariya, C., and Markus, U. I. (2021). Airborne magnetic and radiometric mapping for lithostructural settings and its significance for bitumen mineralization over Agbabu bitumenbelt, southwestern Nigeria. Journal of African Earth Sciences; 180(1): 104222.

[92] Eshanibli, A. S. Osagie, A. U. Ismail, N. A. and Ghanush, H. B. (2021). Analysis of gravity and aeromagnetic data to determine structural trend and basement depth beneath the Ajdabiya Trough in northeastern Libya. SN Applied Sciences, 3(2), Article 228.

[93] Abbas M. I., Abdelhafeez T. H., Hamed T. A., and Rabeh T. (2024). Determining the Depth of Basement Surface and Subsurface Structures at Qarun Lake through Magnetic Data. Annals Geol. Surv. Egypt. XL (2024). pp. 97- 108

[94] Augie, A. I., Ibrahim, A. A., and Olagundoye, B. A., (2022). Aeromagnetic Data Analysis Using Improved Tilt Derivative Technique and 2D Modelling for Mineral Exploration in Parts of Northwestern Nigeria, Mining Science, 29: 179–203.

[95] Alexander, M. J., Pratsch, J. C., and Corine, P. (1998). Under the northern Gulf basin: basement depths and trends. In SEG Technical Program Expanded Abstracts. Society of Exploration Geophysicists; pp. 518–520.

[96] Reid, A.B., Fitzgerald, F., and Mcinemy, P. (2003). Euler Deconvolution of Gravity Data. Society of Exploration Geophysics. SEG 2023 Conferences, Dallas. https://doi.org.10.13140/2.1.3210.0489

[97] Xie, S and Tu, Z. (2015). Holistically-nested Edge Detection. In proceedings of the IEE International Conference on Computer Version, Santiago, Chile. 7th-13th October, 2015.

[98] Xiong, W., Ji, X., Ma, Y., Wang, Y; AlBinHassan, N.M., Ali, M.N., and Luo, Y. (2018). Seismic Fault Detection Workflow with Convolutional Neural Network. Geophysics. 83(1): 97-103.

[99] Zhao, T and Mukhopadhay, P. (2018). Fault Detection Workflow using Deep Learning and Image Processing. In Proceedings of the 2018. SEG International Exposition and Annual Meeting. Anahem, C.A. USA, 16th October, 2018. OnePetrol Richardsong, Texas, USA.

[100] Dzukogi, A.N., Sanusi, Y.A., and Adeyinka, K.S. (2020). Euler Deconvolution and 2D Modelling of Subsurface Structures over Part of Northern Bida and its Surrounding Basement Rocks, North-West Nigeria using Magnetic Method. VIBGYOR International Journal of Earth Sciences and Geophysics. 6(2): 3427-3443. https://doi.org.10.35840/2631-5033/1838; https://vibgyorpublications.org

[101] Tang, Z., Wu, B., Wu, W and Maa, D. (2023). Fault Detection via 2.5D Transformer U-Net with Science Data Preprocessing. Remote Sensing Journal; 15(4): 1039-1049. https://doi.org.10.3390/rs15041039

[102] Ishola, S.A and Ademulegun, M.A. (2025). Geological Charaterization and Depth to Basement Mapping of Magnetic Sources using High-Resolution Aeomagnetic Data: A

Case Study of Ado-Ekiti and Environs (Sheet 244), South-West Nigeria. Unpublished Research Project. Department of Earth Sciences, Olabisi Onabanjo University Ago-Iwoye, South-West Nigeria. 1-131.

[103] Omotoyinbo, Olusoji S. and Okafor, Francis C. (2008). Influence of Rock Mineralogy on Subsurface Water in Ado-Ekiti, Nigeria. African Research Review; 2(2): pp. 175-186

[104] Ajakaiye, D. E. Hall, D. H. Ashiekaa, J. A. and Udensi, E. E. (1991). Magnetic anomalies in the Nigerian continental mass based on aeromagnetic surveys. Tectonophysics; 192(1–2): 211–230. https://doi.org/10.1016/0040-1951(91)90258-T

[105] Ojo, O. J., and Omotose, S. O. (2008). Microfloral assemblage, age and palaeoenvironment of the Upper Cretaceous Patti Formation, Southeastern Bida basin, Nigeria. Journal of Mining and Geology; 44(1): 71-78.

[106] Ajibade, A. C., and Wright, J. B. (1989). The Togo-Benin-Nigeria Shield: Evidence of Crustal Aggregation in the Pan-African Belt. Tectonophysics; 165: 125-129.

[107] Ajayi, A. O., and Akintorinwa, O. J. (2015). Geoelectric investigation of a site for a proposed airport in Ebonyi State, Southeast Nigeria. FUDMA Journal of Sciences; 1(1), 315-320.

[108] Zhang, C., Mushayandebvu, M.F., Reid, A.B., Fairhead, J.D., and Odegard, M.E. (2000). Euler Deconvolution of Gravity Tensor Gradient Data. Geophysics; 65(2): 512-520.

[109] Hood, P. (1965). Gradient Measurements in Aeromagnetic Surveying. Geophysics. 30: 791-802.

[110] Thompson, D.T. (1982). EULDPH-A New Technique for Making Computer-Assisted Depth Estimates from Magnetic Data. Geophysics; 47: 31-37.

[111] Reid, A.B. (1995). Euler Deconvolution Past, Present, and Future, a Review: 65th Annual International Management Society of Exploration Geophysics; Expanded Abstracts. 272-273.

[112] Stanley, J.M and Green, R. (1976). Gravity Gradients and the Interpretation of the Truncation Plate: Geophysics; 41: 1370-1376.

[113] Wilsher, W.A. (1987). A structural Interpretation of the Witwatersrand Basin through the Application of Automated Depth Algorithms to both Gravity and Aeromagnetic Data: M.Sc Dissertation, University of Witwatersrand, South Africa.

[114] Corner, B and Wilsher, W.A. (1989). Structure of the Witwatersrand Basin Derived from the Interpretation of the Aeromagnetic and Gravity Data in Garland, G.D, Ed., Proceedings of Exploration ’87: Third Decennial International Conference on Geophysical and Geochemical Exploration for Minerals and Groundwater: Ontario Geol. Survey; Special Volume. 3: 532-546.

[115] Klingele, E.E., Marson, I., and Kahle, H.G. (1991). Automatic Interpretation of Gravity Gradiometric Data in two dimensions: Verti Grad: Geophysical Prospecting; 39(1): 407-434.

[116] Marson, I., and Klingele, E.E. (1993). Advantages of using the vertical gradient of Gravity for 3D Interpretation: Geophysics; 58: 1588-1595.

[117] Fairhead, J.D., Bennett, K.J., Gordon, R.H., and Huang, D. (1994). Euler: Beyond the Black Box: 64th Annual International Management Social Exploration Geophysics; Expanded Abstracts. 422-424.

[118] Huang, D., Gubbins, D., Clark, R.A., and Whaler, K.A. (1995). Combined Study of Euler’s Homogeneity Equation for Gravity and Magnetic Field: 57th Conference and Technical Exhibition. European Association of Exploration Geophysics; Extended Abstracts. 144.

[119] Mushayandebvu, M.F., Van-driel, P., Reid, A.B., and Fairhead, J.D. (2001). Magnetic source parameters of two-dimensional structures using extended Euler deconvolution. Geophysics; 66(1): pp. 814-823.

[120] Verduzco, B., Fairhead, J. D., Green, C. M. and MacKenzie, C. (2004). New insights into magnetic derivatives for structural mapping. The Leading Edge; 23(2): 116–119

[121] Awoyemi, M.O., Arogundade, A.B., Falade, S.C., Ariyibi, E.A., Hammed, O.S., Alao, O.A and Onyedim, G.C. (2016). Investigation o Basement Fault Propagation in Chad Basin of Nigeria using High Resolution Aeromagnetic Data. Arabian Journal of Geosciences; 9(6): 453.

[122] Emujakporue, G., Ofoha, C.C., and Kiani, I. (2017). Investigation into the Basement morphology and Tectonic lineament using Aeromagnetic Anomalies of parts of Sokoto Basin, Northwestern Nigeria. Egyptian Journal of Petroleum; 27(4): 103. https://doi.org.10.1016/j.ejpe.2017.10.003

[123] Adewumi, T. T., and Salako, K. A. (2017). Qualitative interpretation of aeromagnetic data for mineral potential assessment in Nasarawa State, north-central Nigeria. Nigerian Journal of Mining and Geology; 53(1): 45–58.

[124] Ekwueme, O.U., Obiora, D.N., Igwe, E.A., Abangwu, J.U. (2018). Study of Aeromagnetic Anomalies of Idah and Angba Areas, North-Central using High-Resolution Aeromagnetic Data. Modelling Earth Systems and Environment; 4(2): 461-474.

[125] Okpoli and Akingboye, 2019;

[126] Arogundade, A.B., Hammed, O.S., Awoyemi, M.O., Falade, S.C., Ajama, O.D., Olayode, F.A., Adebayo, A.S and Olabode, A.O. (2020). Analysis of Aeromagnetic Anomalies of Parts of Chad-Basin, Nigeria using High Resolution Aeromagnetic Data. Modeling Earth Systems and Environment; 6(3): 1545-1556.

[127] Salawu et al., 2020; Salawu, N. B. Orosun, M. M. Adebiyi, L. S. and Abdulraheem, T. Y. (2020). Existence of subsurface structures from aeromagnetic data interpretation of the crustal architecture around Ibi, Middle Benue, Nigeria. SN Applied Sciences; 2(3): Article 2230.

[128] Layade, G.O., Adewumi, O., Makinde, V and Bada, B. (2020). Estimation of Depth to Bouguer Anomaly Sources using Euler Deconvolution Techniques. RMZ-M & G2020. 671: 185-195. https://doi.org.10.2478/RMZM&G-2020-0016

[129] Tawey, J. G., Olasehinde, P. I., Olorunfemi, M. O., and Akinluyi, F. O. (2020). Aeromagnetic investigation of subsurface structures and solid mineral potential in north-central Nigeria. Journal of African Earth Sciences; 168: 103845.

[130] Falufosi and Osinowo, 2021; Falufosi, M. O., and Osinowo, O. O. (2021). Evaluation of basement topography and structures in the Dahomey Basin and surrounding environs of Southwestern Nigeria, using satellite gravity data. NRIAG Journal of Astronomy and Geophysics; 10(1): 333-346.

[131] Kahoul, S., Sidek, A., Eshanibli, A. S., Trepil, F., Jaafar, M. Z., Hassan, M., and Ghanoush, H. (2022). Identifying fault system and basement depth using aeromagnetic data beneath the Jahamah Platform, NE Sirt Basin, Libya. Acta Geodynamica et Geomaterialia, 19(2), 155–166.

[132] Akintoye, S.O., Adagunodo, T.A., Oladapo, M.I., Mimoh, E.A., Adebiyi, S.J., and Olayinka, A.I (2023). Many Gravity Maps over Nigeria including the Theoretical Gravity Map, Absolute Gravity Map and Bouguer Gravity Anomaly Map to the Geoid . Journal of Geophysics and Engineering; 20(3): 455-470. https://doi.org.10.1093/jge/gxac055

[133] Edunjobi, S. O., Osinowo, O. O., and Adewumi, T. A. (2021). Estimation of Depth to Magnetic Basement in Ekiti State, Southwestern Nigeria from Aeromagnetic Data Using Spectral Analysis Technique. International Journal of Research and Innovation in Applied Science; 6(4): 1-7.

[134] Layade, G. O., Ajadi, J. A., Olatunji, S., and Imoukhuede, O. B. (2023). Use of Airborne Radiometric Data for Bitumen Exploration in Agbabu Area, Southwestern, Nigeria. IOSR Journal of Environmental Science, Toxicology and Food Technology, 12(2), 09-15.

[135] Layade, G.O., Edunjobi, H.O, and Ajayi, K.D. (2024). Lineament Qualitative Interpretation and Depth Evaluation of Potential Field Signatures in the Abeokuta Region, Southwestern Nigeria. Journal of the Earth and Space Physics; 49(4): 231-239.

[136] Ishola, S.A and Ademulegun, M.A. (2025). Geological Characterizations and Depth to Basement Mapping of Magnetic Sources using High-Resolution Aeromagnetic Data: A Case Study of Ado-Ekiti and Environs (Sheet 244), South-West Nigeria. Unpublished B.Sc Degree Project, Department of Geology, Olabisi Onabanjo University, Ago-Iwoye. pp. 14-17

[137] Babylon, O.B. (2019). Tectonic and structural analysis of the migmatitic gneiss-quartzite complex of Ilorin area from aeromagnetic data. NRIAG Journal of Astronomy and Geophysics; 8(1): pp. 22-23. https://doi.org.10.1080/20909977.2019.1615795

[138] El-Bohoty, M., Khalil, A., Hussain, W., El-kotb, A., Awad, A., and Khalifa, M. (2021). Geophysical studies of subsurface structures of the area surrounding the new part of Jarjob in El-Negila-Massa Matruh using magnetic data. NRIAG Journal of Astronomy and Geophysics; 10(1): pp. 456-471. https://doi.org.10.1080/20900977.2021.1907963

[139] Nagy, D. (1966). The Gravitational Attraction of a Right Rectangular Prism. Geophysics; 31: 362-371.

[140] Nagy and Fury (1990). Nagy, D. and Fury, R.J (1990). Local Geoid Computations from Gravity using the Fast Fourier Transform Technique: B. Geodesique. 64: 283-294.

[141] Forsberg, R. (1984). A study of Terrain Reductions, Density Anomalies and Geophysical Inverse Methods in Gravity Field Models. Department of Geodetic Science and Surveying Report; Ohio State University. Report 355.

[142] Ekwok, S.E., Achadu, O.M., Akpan, A.E., Eldosouky, A.M., Ufuafuonye, C.H., Abdelrahman, K., and Gomez-Ortiz, D. (2022). Depth estimation and basement rocks in the Bornu Basin, North-West Nigeria using High Resolution Airborne Magnetic Data. MDDP Minerals; 12(3): pp. 445-462. https://doi.org.10.3390/min12030285285

[143] Steenland, N.C. (1968). Discussionon the Geomagnetic Gradiometer by H.A Slack, V.M. Lynch, and L.Langan (Geophysics, 1967, 877-892). Geophysics 33:680-683.

[144] Barnett, C.T. (1976). Theoretical modeling of the magnetic and gravitational fields of an arbitrarily shaped three-dimensional body. Geophysics; 41:1353-1364

[145] Schwarz, K.P., Sideris, M.G., and Forsberg, R. (1990). The use of FFT Techniques in Physical Geodesy: Geophysical Journal International; 100: 485-514.

[146] Zhang, C. and Sideris, M.G (1996). Ocean Gravity by Analytical Inversion of Hotine's Formula.Marine Geodesy. 9: 115-136.

[147] Zhang, C. (1995). A General Formula for Gravimetric Transformations by the use of Convolution and Deconvolution Techniques. Journal of Geodesy. 70: 51-64.

[148] Werner, S. (1953). Interpretation of Magnetic Anomalies of Sheet like Bodies. Sveriges Geologist Under SerC.C, Arabok. 43(6): 4-7.

[149] Srivatava, R.P. (2004). Determination of Magnetic Basement using Werner Deconvolution. 5TH Conference and Exposition on Petroleum Geophysics, Hyderabad, 2004. India. Pp. 953-956.

[150] Hartman, D.R., Teskey, D.J and Preidberg, J.L. (1971). A system for Rapid Digital Aeromagnetic Interpretation. Geophysics; 36(5): 891-918.

[151] Jain, 1976;

[152] Ku, C.C and Sharp, J.A. (1983). Werner Deconvolution for Automatic Magnetic Interpretation and its Refinement using Marquardt's Inverse Modeling. Geophysics; 48(6): 754-774.

[153] Malleswara-Rao, M.M., Lakshminarayana, S., Murthy, K.S.R and Subrahmanyam, A.S. (1993). Two ComputerPrograms for the Analysis of Marine Magnetic Data. Computer and Geosciences. 19(5): 657-672.

[154] Sarma, K.V.L.S., Ramana, M.N., Murthy, G.P.S., Subrahmanyam, V., Krishna, K.S., Chaubey, A.K., Mallaswara-Rao, M.M and Narayana, S.L. (1994). Application of Inversion Techniques on Marine Magnetic Data-Andaman Shelf, Journal of Geological Society of India; 44(1): 73-78.

[155] Thakur, N.K., Gangadhara-Rao, T., Ramesh-Khanna and Subrahmanyam, C. (2000). Magnetic Basement in the Bay of Bengal through Werner Deconvolution. Marine Geology; 162: 599-605.

[156] Martins, O.E., Mosto, O.K., and Ifeanyi, O.A. (2021). Aeromagnetic interpretation of basement structure and architecture of the Dahomey basin, Southwestern Nigeria. NRIAG Journal of Astronomy and Geophysics; 10(1): pp. 93-109. https://doi.org.10.1080/2099977.2021.1880817

[157] Radhakrishna-Murthy, I.V., Swamy, K.V., and Rama-Rao, P. (2000). Use and Abuse of Werner deconvoluion Technique. Journal of India Geophysical Union; 4(2): 97-102.

[158] Rao, B.S.R., Radhakrishna-Murthy, I.V. and Visweswara-Rao, C. (1973). A Direct Method of Interpreting Gravity and Magnetic Anomalies: The case of a Horizontal Cylinder, PAGEOPH. 102(11): 67-72.

[159] Sudhakar, K.S., Rao, P.R and Radhakrishna-Murthy, I.V. (2004). Journal of India Geophysical Union; 8(3): 179-183.

[160] Radhakrishna-Murthy, I.V. (1998). Gravity and Magnetic Interpretation in Exploration Geophysics. Geological Society of India, Banglore, India

[161] Keating, P. (1995). A simple technique to identify magnetic anomalies due to Kimberlie pipes: exploration. Mining Geology; 4(1): pp. 121-125.

[162] Sylvester, E. E., Okpoli, E., & Oladejo, O. P. (2018). Interpretation of aeromagnetic data over some parts of Mambilla Plateau, Taraba State. International Journal of Physical Sciences, 13(4), 33-42.

[163] Edunjobi, H.O., Layade, O.G., Makinde, V., Bada, B.S., Ogunbayo, A.F., and Atunrase, K.A. (2023). Qualitative Interpretation of High Resolution Aeromagnetic Data of Abeokuta Metropolis for Geological Characterization. Results in Geophysical Sciences. 15(1): 101-128.

[164] NGSA. (2005). Nigerian Geological Survey Agency. Airborne Geophysical Digital Data Dissemination Guidelines. 22-25.

[165] NGSA. (2005). Nigerian Geological Survey Agency. High-Resolution Airborne Geophysical Survey. NGSA Bulletin. pp. 16

[166] Tsokas, G.N and Papazachos, C.B (1992). Two-dimensional inversion fitters in magnetic prospecting: Application to the exploration for buried antiquities. Geophysics; 57(1): pp. 1004- 1013. https://doi.org.10.1190/1825939

[167] Arekumo, T. (2023). Applying Geophysical Method for Investigation of the Depth of the Mineralization Potential of Ikogosi and Environs Using Aeromagnetic Data. World Scientific News; 184: 75-88.

[168] El-Dawn, M.G., Tianyouw, L., Hui, S., and Dopeng, L. (2004). Depth estimation of 2D magnetic anomaly sources by using Euler deconvolution method. American Journal of Applied Science; 1(3): pp. 209-214. https://doi.org.10.3844/ajassp.2004.209.214

[169] Ogah, A.J and Abubakar, F. (2024). Solid Mineral Potential Evaluation using Integrated Aeromagnetic and Aeroradiometric Datasets. Scientific Reports; 14(1): 167. https://doi.org.10.1038/s41598-024-52270-6

[170] Okpoli, C.C and Oladunjoye, M.A (2017). Precambrian Basement Architecture and Lineaments Mapping of Ado-Ekiti Region using Aeromagnetic Dataset. Geosciences Research. 2(1): 27-45. https://doi.org.10.22606/gr.2017.21005

[171] Ostrowski, J. A., Pilkington, M., and Morris, W. A. (1993). Werner deconvolution for variable altitude aeromagnetic data. Geophysics, 58(10), 1481-1490.